Intergovernmental Oceanographic Commission technical series

42

Calculation of New Depth Equations for Expendable Bathythermographs Using a Temperature-Error-Free Method (Application to Sippican/TSK T-7, T-6 and T-4 XBTs)

by
K. Hanawa
Tohoku University, Dep. of Geophysics,
Sendai 980, Japan.

P. Rual
ORSTOM, Surtropac group
Noumea, New Caledonia.

R. Bailey
CSIRO, Division of Oceanography
Hobart, Tasmania 7001, Australia.

A. Sy
Bundesamt fuer Seeschiffahrt und Hydrographies
Hamburg 36, Germany

and
M. Szabados
NOAA/NOS-OOES
Silver Spring, MD 20910-3233, USA.

members of the IOC/IGOSS Task Team
on Quality Control of Automated Systems

UNESCO 1994

The designations employed and the presentation of the material in this publication do not imply the expression of any opinion whatsoever on the part of the Secretariats of UNESCO and IOC concerning the legal status of any country or territory, or its authorities, or concerning the delimitations of the frontiers of any country or territory.

Abstract

A new depth-time equation for Sippican and Tsurumi-Seiki (TSK) T-7, T-6, and T-4 type expendable bathythermographs (XBTs) is presented based on the results of an internationally co-ordinated set of controlled XBT-CTD comparison experiments geographically distributed over as many different oceanic water masses as possible. A newly developed temperature-error-free method is applied to the data set to obtain the time-depth pairs necessary for the calculation of the individual depth-time equations by the method of least squares. The accuracies in depth were found in general to be outside of the manufacturers' specified accuracies. The mean depth-error for the T-7 type of probe was found to be about +25m at 750m, whereas the manufacturers' depth-accuracy specification at 750m is only ± 1 Since the T-4/T-6 and the T-7 data sets were found not to be statistically different at the 95% confidence level, a unique new Sippican-TSK T-4/T-6/T-7 depth-time equation, whose coefficients are the means of the individual depth-time equation coefficients, is given (at a 95% confidence level) by:

$$Z = (6.691 \pm 0.021)\, t - (2.25 \pm 0.30)10^{-3} t^2,$$

where Z is the new corrected XBT depth in metres at the elapsed time t in seconds. It replaces the manufacturers' equation ($Z_m = 6.472\, t - 2.16\, 10^{-3} t^2$). The new equation reduces the mean depth-errors to less than ± 1m in the range 0-800m. However the individual scatter of the probes is much larger than the manufacturers' specifications. The observed scatter at 3 standard deviations (99.7°/0) is approximately ± 10m at 10Om and $\pm$ 25m at 800m. The relationship between the scatter of the individual quadratic depth-time equation coefficients and the depth-error is discussed. It is shown that depth-differences between respective depth-time equations can be small, even if the two coefficients of the equations have apparently very different values. The effect of the region, of the onboard equipment or of the manufacturer, is also discussed and generally found not to be statistically significant, i.e. smaller than the above probe to probe scatter. An approximate linear correction formula is determined for correcting (with a maximum error of ± 0.1m) the depths recorded using the manufacturers' original depth-time equation (z_m). It is given by : $Z_1 = 1.0336\, z_m$.

Until an international mechanism is established to implement the general use of the new equation, it is of the utmost importance not to use the new T-4/T-6/T-7 equation when archiving or exchanging XBT data. The mixing of data in the data archives must be absolutely avoided.

Table of Contents

(i v)

1. Introduction

In recent times expendable oceanographic probes, in particular expendable bathythermographs (XBTs), have been a significant component of many large scale oceanographic research programmes, such as the Tropical Ocean Global Atmosphere (TOGA) Programme and the World Ocean Circulation Experiment (WOCE). These types of probes can be launched whilst underway from ships-of-opportunity, such as merchant vessels, enabling large scale repeated coverage of the major ocean basins. As the importance of the ocean's role in the climate system has become increasingly acknowledged, so has the need to observe and monitor the variability of the major components of the ocean related to the climate system. This is being successfully achieved through the use of expendable probes. These probes will no doubt be heavily relied upon in future operational oceanographic programmes such as the proposed Global Ocean Observing System (GOOS).

Although the achieved accuracies of XBTs were sufficient for most earlier studies, the relatively small changes induced in the ocean by climate change and interannual variability have resulted in a growing need to utilise these instruments to the limits of their accuracies. This has inevitably led to a number of studies on the specified accuracies of the instruments.

The possibility of an error in the depth-time equation for XBTs was first reported by Flier] and Robinson (1977). The depth of the XBT at any particular instant is not directly measured, but is inferred from an assumed fall rate of the probe. As most studies involve the merging of XBT and conductivity-temperature-depth (CTD) sensor data, any apparent systematic differences between the depths of isotherms obtained by XBTs and CTDs in the same area may create a biased representation of the temperature fields. When CTD and XBT measurements are conducted along an observational transect, a pseudo-undulation of the isotherms appears in the vertical temperature cross-section. This is due to the depth error in the XBT data, and its existence has already been pointed out by several authors (e.g., Flier] and Robinson, 1977; Seaver and Kuleshov, 1982; Heinmiller *et al.,* 1983). Several investigators have since estimated revised depth-time (fall rate) equations for the XBT using a number of different techniques (McDowell, 1977; Heinmiller *et al.,* 1983; Green, 1984; Hanawa and Yoritaka, 1987; Henin, 1989; Gould, 1990; Singer, 1990; Sy and Ulrich, 1990; Hanawa and Yoshikawa, 1991; Hallock and Teague, 1992, Hanawa and Yasuda, 1992). In addition, Green (1 984) provides a detailed description of the hydrodynamics of XBTs.

The Integrated Global Ocean Services System (IGOSS) Task Team on Quality Control for Automated Systems (TT/QCAS) initiated an international effort, by dedicated TOGA and WOCE scientists within the team who work with XBT data, to conduct further XBT/CTD comparison tests under controlled experimental conditions. The aim was to address some of the ambiguities of the earlier studies, and to develop accurate new equations for universal use in the community. The probes evaluated were the commonly used Sippican and Tsurumi-Seiki (TSK) T-7 (760m), T-6 (460m) and T-4 (460m) types of XBT, all of which use the same manufacturers' depth-time equation. The co-investigators' initial individual results can be found in a report of the Intergovernmental Oceanographic Commission (1 992). The individual new depth-time equations were generally very similar. It was therefore decided to combine all data sets collected by the co-investigators, and to apply the best available depth-error estimation technique (a modification of the independently developed temperature-error-free method of Hanawa and Yasuda, 1992, and of Rual, 1991). This is the focus of the present study.

New depth-time equations are calculated independently for both the T-7 and T-4/T-6 types of XBTs to check for possible differences in the fall rate characteristics of the different types of probes. Then a new unique reference depth-time equation for the combined data set is determined. The possible influences on the fall rates by different water masses, onboard recording equipment, and probe manufacturers are also examined. The scatter of the fall rates is compared to the manufacturers' specifications. A review is made of the results obtained by previous investigators, and their results are compared to the new depth-time equation. Finally, the necessity for evaluations of the other types of probes and recommendations for the use of new depth-time equations are discussed.

2. XBT/CTD Comparison Experiment

2.1 Probe types and manufacturers

The results presented in this paper apply to Sippican or TSK T-7 (760m), T-6 and T-4 (460m) models of XBT probes, all of which use the same manufacturers' depth-time equation. The nose cones of the T-4 and T-6 XBTs are manufactured heavier than those of the T-7 to match the T-7 in overall weight (more wire on the probe spool), in fall rate characteristics , and hence in the depth-time equation. Since the only difference between the T-6 and T-4 types of XBT is the amount of wire on the ship spool so as to allow the T-4 probe to be dropped from faster vessels, these two types of probes are not distinguished between for this study. XBTs made by TSK, manufactured under a Sippican licence, should be identical to the original Sippican probes. Some Sippican Deep Blues (760m) were also tested, but as their probes are identical to the probes of the T-7, they are not distinguished between for this study and hereafter will be considered as T-7.

2.2 Locations and descriptions of the data sets

Between 1985 and 1992, XBT/CTD comparison experiments were independently carried out by five institutions and by one manufacturer (see Table 1). The comparison data were classified according to the type of XBT, type of data recorder, experimental site location and date of the experiment. These data sets are given individual identifiers. For example, C7A is the first data set collected by CSIRO using T-7 probes. For the present analysis, a total of 161 T-7 and 211 T-4/T-6 profiles were collected by these institutions.

In Fig. 1 are shown the locations where the XBT/CTD comparison experiments were conducted. Temperature-salinity (T-S) relationships, extracted from climatological data (Levitus, 1982), are displayed in Fig. 2 for each region. An hundred-metre mark has been added to each curve to show the extent of the surface waters. The non-shaded area represents the open-waters T-S field of the World Ocean, it is limited by the salinity extrema found in the Levitus Atlas (1982) between 50m and 800m, and between 30 and 39 psu. The surface levels and the extreme salinities have been excluded as they may not be representative of the open ocean; they may be 'polluted' by ice melt, heavy rainfall, river outflow or evaporation in semi-closed gulfs.

It can be concluded that the comparison data used in the present study are distributed over various oceans and accordingly cover various water masses (S = 34 to 37 psu, T = 5°C to 30°C). The comparison experiments were made in several different regions so as to specifically assess the possible influence of the density and viscosity structures on the XBT fall rate (Seaver and Kuleshov, 1982). Only open ocean conditions have been sampled. Extreme oceanic conditions such as the Arctic and Antarctic oceans, the Red Sea, the Baltic Sea and the Mediterranean Sea, were not included due to lack of opportunity to obtain measurements in these areas.

2.3 Experimental procedures

The controlled experimental procedures are as follows:

All XBT data are evaluated relative to a field standard, the conductivity-temperature-depth (CTD) profiler (Table 1). Generally, the CTD profilers were calibrated before and after each voyage of the research vessels involved, and the calibration results were applied to the CTD data before analysis. Therefore CTD data errors are at least an order of magnitude smaller than XBT data errors and, for this study, will be considered as negligible.

A number of different digital XBT recorders were used to collect the XBT data (Table 1). Each XBT recorder underwent a calibration check before and after each voyage. No strip chart recorders were used for this experiment as this type of recorder may include additional depth-errors in the readings due to variations in the speed of the chart-roller mechanism.

Table 1 Summary by region of the CTD-XBT comparison experiments for T-7 XBTs (Table 1a), T-4/T-6 XBTS (Table 1b). Field areas are shown on Fig. 1. Columns 3, 4 and 5 indicate, respectively, the number of probes launched, the number of temperature profiles having a certain number of 'good' depth-differences: at least 1/3 or 2/3 of the maximum number of depth-differences (27 for T-7 and 15 for T-4/T-6, see Eq. 3 in *step* 3 of the method). The last 9 columns are respectively: i) the mean A and B coefficients of the regional depth-time equations; *ii)* the maximum absolute depth-error (in metres and in percentage) to the reference T-4/T-6/T-7 equation (9), down to 800m (T-7) or to 450m (T-4/T-6); *iii)* the correlation coefficient between A and B; *iv)* the standard deviations of the mean and of the individual coefficients.

TABLE 1a: Summary of CTD-XBT comparison experiments for T-7 XBT's (161 probes)

Region	Data set	Nb. of XBT	Profiles [9-27] pts	Profiles [18-27] pts	Manu-facturer	Field Experiment Date	Field Experiment Institution	XBT recorder	CTD profiler	A	B (10⁻⁵)	Max Depth-error metre	Max Depth-error %	correl. coef. (AB)	σ_A 10⁻³	σ_B 10⁻⁵	σ_a 10⁻³	σ_b 10⁻⁵
NW Pac. (nwp, 1)	Total	37	34	33	TSK	1985-87-91	TOHOKU	-	NB IIIb	6.723	253	0.9	0.24	0.93	24	18	139	103
	T7A	15	12	11		12/85		ORI										
	T7C	8	8	8		09/87		Z-60-II										
	T7D	10	10	10		06/89		Z-60-II										
	T7E	4	4	4		01-02/91		Z-60-II										
NW Trop.Pac. (nwtp, 2)	T7B	9	9	9	TSK	02/1987	TOHOKU	ORI	NB IIIb	6.652	201	-1.6	-0.30	0.78	20	27	61	81
W Equat.Pac. (wep, 4)	Total	21	16	16	Sippican	1989-91-92	ORSTOM	Argos	SBE-9	6.680	226	-1.5	-0.19	0.85	28	23	110	94
	O7A	10	10	10		06-07/89												
	O7B	4	3	3		12/89												
	O7C	5	1	1		03-04/91												
	O7D	1	1	1		01/92												
	O7E	1	1	1		03/92												
SW Trop.Pac. (swtp, 5)	Total	24	24	23	Sippican	1989-92	ORSTOM	Argos	SBE-9	6.672	225	-2.4	-0.30	0.62	18	14	86	69
	O7A	12	12	11		06-07/89												
	O7B	8	8	8		12/89												
	O7D	4	4	4		01/92												
Tasman Sea (6)	C7A	12	11	6	Sippican	08-09/1989	CSIRO	Mk-9	NB	6.747	200	10.9	1.36	0.84	69	38	169	93
SE Indian (sei, 3)	Total	21	19	13	Sippican	1987	CSIRO	-	NB	6.666	224	-3.0	-0.37	0.94	29	19	105	68
	C7B	8	7	4		04/87		Mk-9										
	C7C	7	7	6		04/87		SA-810										
	C7D	3	3	2		11/87		Mk-9										
	C7E	3	2	1		11/87		Mk-9										
NW Trop.Atl. (nwta, 8)	Total	25	24	15	Sippican	1988-91	-	-	NB III	6.854	324	6.7	1.25	0.54	19	15	75	58
	N7A	7	7	6		07/88	NOAA/NOS	Mk-9										
	N7B	6	6	5		07/88	NOAA/NOS	Argos										
	S7A	12	11	4		06-07/91	SIPPICAN	Mk-9										
NE Atlant. (nea, 9)	B7A	12	10	10	Sippican	09/1991	BSH	Mk-12	NB III	6.561	179	-9.1	-1.13	0.92	34	30	108	93
TOTAL		161	147	125			New T-7 Equation (7)			6.701	238	-0.8	-0.10	0.85	12	8	130	91

TABLE 1b: Summary of CTD-XBT comparison experiments for T-4/T-6 XBT's (211 probes)

Region	Data set	Nb. of XBT	Profiles [5-15] pts	Profiles [10-15] pts	Manu-facturer	Field Experiment Date	Field Experiment Institution	XBT recorder	CTD profiler	A	B (10⁻⁵)	Max Depth-error metre	Max Depth-error %	correl. coef. (AB)	σ_A 10⁻³	σ_B 10⁻⁵	σ_a 10⁻³	σ_b 10⁻⁵
NW Pac. (nwp, 1)	Total	17	17	17	TSK	1989-92	TOHOKU	Z-60-II	NB IIIb	6.566	164	-5.7	-1.27	0.97	31	52	129	213
	T6A	9	9	9		06/89												
	T6B	8	8	8		04/92												
W Equat.Pac. (wep, 4)	Total	80	66	54	Sippican	1989-91-92	ORSTOM	Argos	SBE-9	6.656	194	-0.9	-0.26	0.90	33	60	245	439
	O4A	16	12	12		12/89												
	O4B	11	11	9		08/91												
	O4C	21	15	9		09/91												
	O4D	32	28	24		02-03/92												
SW Trop.Pac. (swtp, 5)	Total	52	41	34	Sippican	1989-91-92	ORSTOM	Argos	SBE-9	6.708	266	-0.8	-0.17	0.87	36	62	209	360
	O6A	2	1	1		12/89												
	O4B	8	8	7		08/91												
	O4C	5	3	2		09/91												
	O4D	37	29	24		02-03/92												
NW Trop.Atl. (nwtp, 2)	Total	41	40	40	Sippican	1988-91	-	-	NB III	6.810	281	5.5	1.23	0.76	14	21	86	133
	N6A	7	7	7		07/88	NOAA/NOS	Mk-9										
	N6B	13	13	13		07/88	"	Argos										
	N4A	7	6	6		07/88	"	Mk-9										
	N4B	7	7	7		07/88	"	Argos										
	S4A	7	7	7		06-07/91	SIPPICAN	Mk-9										
Bahamas (7)	N4C	21	21	15	Sippican	02/1992	NOAA/NOS	Mk-9	NB III	6.514	061	-4.8	-1.35	0.93	32	53	123	205
TOTAL		211	185	160			New T4/T6 Equation (8) :			6.683	215	-0.2	-0.06	0.86	16	26	206	329

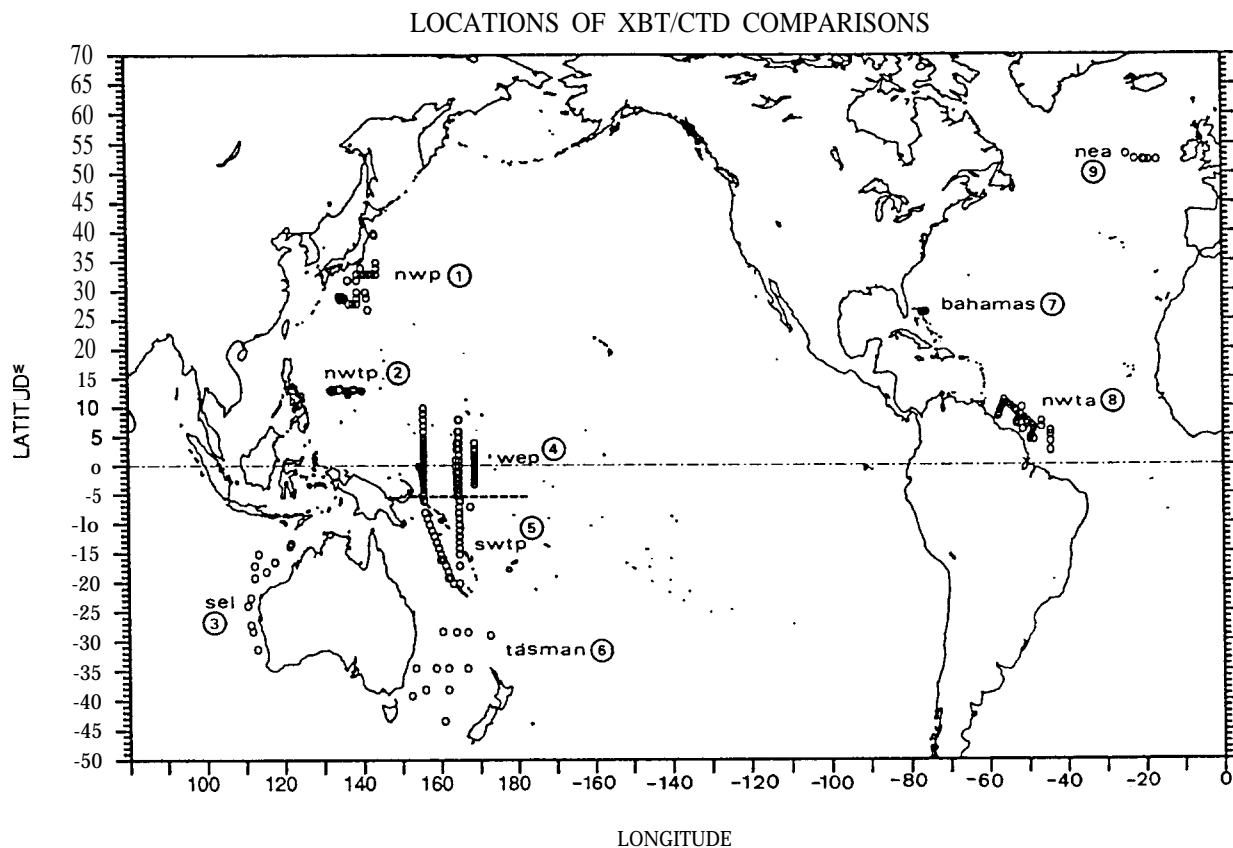|			
BSH	: Bundesamt fur Seeschiffahrt und Hydrographie, (Germany)	Mk-9	: Sippican Mark 9
		Mk-12	: Sippican Mark 12
CSIRO	: Commonwealth Scientific and Industrial Research Organisation, (Australia)	SA810	: Bathy-Systems model SA-810
NOAA/NOS	: National Oceanic and Atmospheric Administration, (USA)	Argos	: CLS-Argos / Protecno XBT-ST model 1 and 2
ORSTOM	: Institut Français de Recherche Scientifique pour le Développement en Coopération, (France)	ORI	: Ocean Research Institute, Tokyo University
TOHOKU	: Tohoku University, (Japan)	Z-60-II	: Murayama Denki
		TSK	: Tsurumi Seiki
		NB	: Neil Brown
		NB III	: Neil Brown model 3
		NB IIIb	: Neil Brown model 3b
		SBE-9	: SeaBird model 9

LOCATIONS OF XBT/CTD COMPARISONS

Figure 1. Locations where the CTD-XBT comparison experiments were conducted (See also Table 1a and 1b.). The dashed line at 5°S in the western Pacific shows the limit between the *wep* and *swtp* data sets.
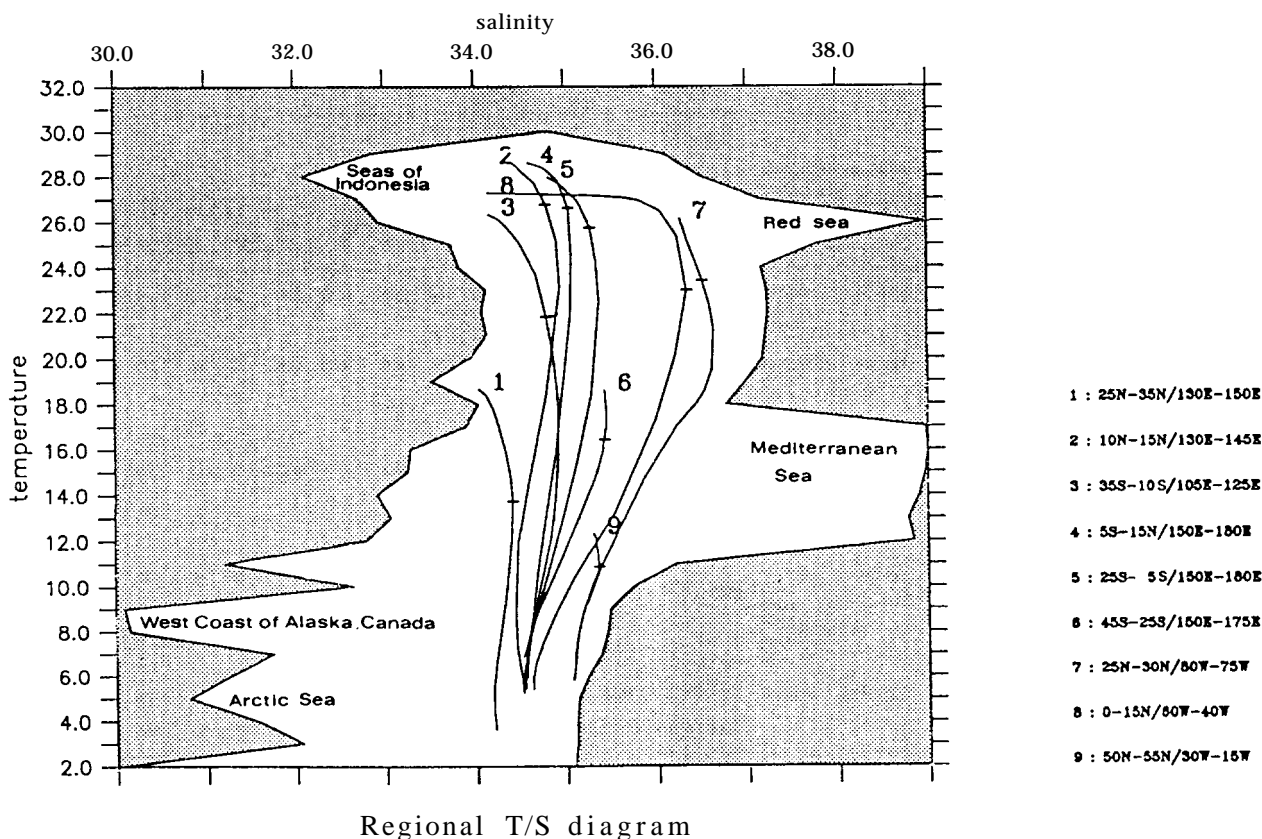

Regional T/S diagram

Figure 2. Temperature-salinity (T-S) diagrams from climatological data (Levitus, 1982). Curves 1 to 9 represent the field areas of the comparison experiment (see Fig. 1 and Table 1). A hundred-metre mark has been added to each curve. The shaded area limits the T-S field of the world's open oceans defined by the salinity extrema found in the Levitus Atlas: between 50m and 800m and between 30 and 39 psu.

A "side by side" XBT/CTD comparison was the main improvement in the field procedures used in this study compared to most of the previous investigators' studies. As far as possible, XBTs were dropped during the descent of the CTD so that, at least at some depth, the instruments were coincident in depth. This was in attempt to eliminate as much as possible depth-differences due to temperature-field variations in time or space (e.g. internal waves). Generally, XBTs were dropped within 10-15 minutes of the start of descent of the CTD, for the coincidence to be within the thermocline. Previous investigators had not necessarily compared XBTs that were as close in time as possible (or indeed at precisely the same location) to the CTD.

3. Temperature-Error-Free Method to Calculate an XBT Depth-Time Equation

Provided that the on board XBT equipment is working correctly, it is considered that there are two main error-sources in XBT data: *i)* Depth-errors due to an inaccurate depth-time equation for the fall rate of the probes; *ii)* Temperature errors due to the scatter of thermistor responses and inaccuracies in the conversion of thermistor resistance to temperature. In this study we will only examine the depth-errors associated with inaccuracies in the fall rate equation.

For a given type of probe, the depth-time equation provided by the XBT manufacturers is of the form:

$$z_\mathrm{m} = a_\mathrm{m}t - b_\mathrm{m}t^2 \tag{1}$$

where z_m is the depth and t *is* the elapsed time in seconds starting when the probe hits the surface; a_m and b_m are positive constants. The linear coefficient is a function of the hydrodynamic characteristics of the probe in the water, while the quadratic coefficient is a function of the change in mass of the probe (unreeling of the wire) and of the change with depth of the water characteristics (density and viscosity gradients; see Green, 1984).

3.1. The Method

Hanawa and Yoritaka (1987) and Hanawa and Yoshikawa (1991) first developed a temperature-error-free method for determining errors in the depth-time equation. The essence of the method is that comparison to the field standard should be made not for the absolute temperature profiles but for the temperature gradient profiles. This is because temperature errors are directly related to depth errors, and bias-like temperature errors can be eliminated by using the temperature gradient information.

The detection method adopted for the depth-error in the present analysis is an extension of this method. It was first independently developed by Hanawa and Yasuda (1992) and Rual (1991), and is further simplified and modified here for better accuracy. In this section, each step of the procedure is described and general remarks are made on the technique.

3.1.1 *Procedures for depth-error detection*

The detection procedures used in the present analysis for obtaining depth-errors are as follows:

- *step 1, One metre-interval data* . The one metre-interval data are calculated using a linear interpolation scheme for both raw CTD and XBT temperature data. Here, the CTD pressure is converted into depth by using the approximate equation (2) of Hanawa and Yoritaka (1987), calculated for a *sigma-t* of 27.5:

$$z_\mathrm{ctd} = 0.993\, p_\mathrm{ctd} \tag{2}$$

where z_ctd is the CTD depth in metres and p_ctd is the CTD pressure in decibars. The XBT depths, z_m, are calculated using the depth-time equation provided by the XBT manufacturer(1)
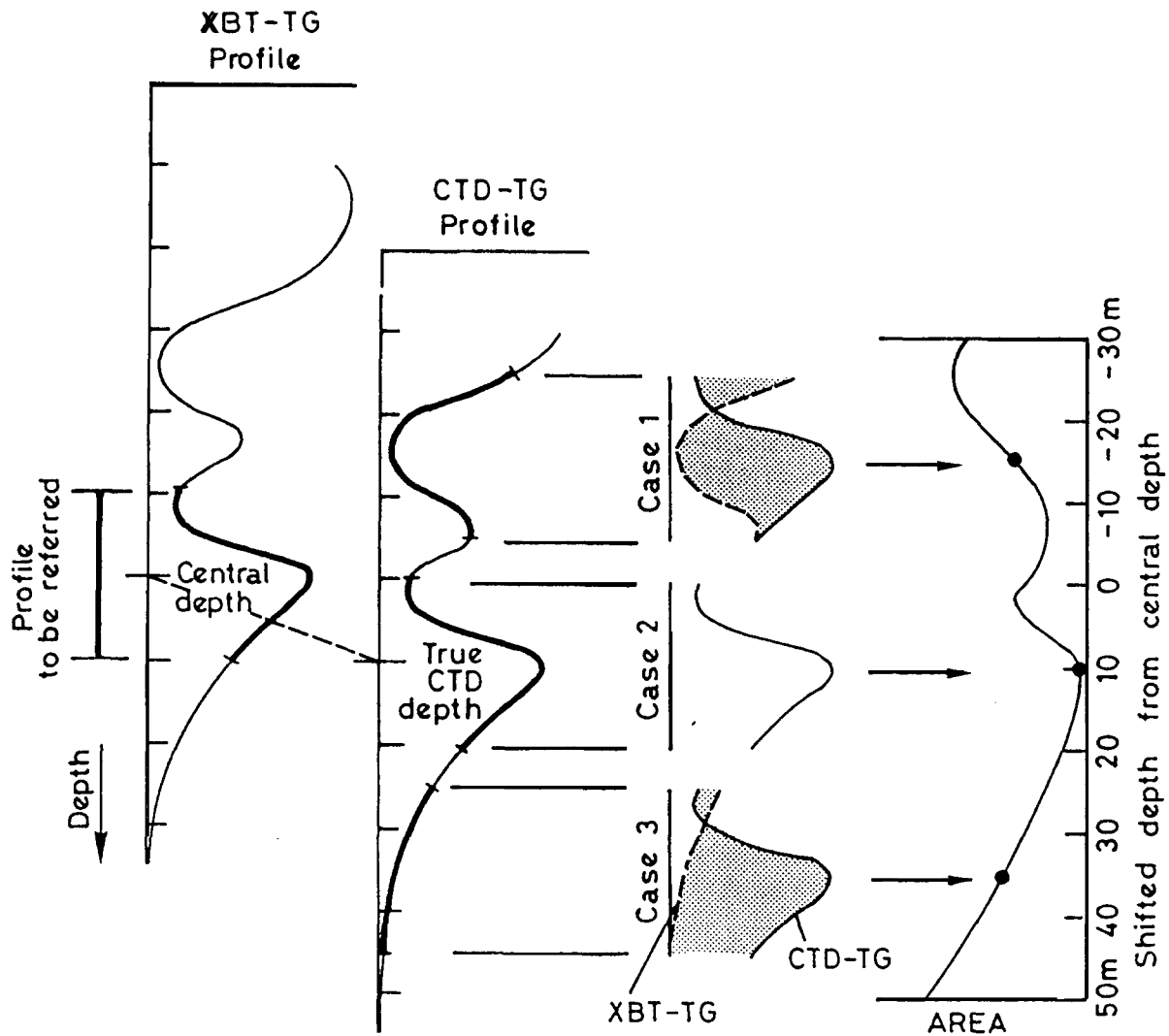
Figure 3.   Explanatory picture of the detection method adopted to determine the XBT depth-error (adapted from Hanawa and Yasuda, 1992). See section 3. I .1, *step* 4, in the text for details. In this figure, only three examples are shown. Since the area has its minimum value in Case 2, its shifted CTD central depth is the actual depth of the reference central XBT point, and its depth-shift (+10m) is regarded as the depth correction of the XBT data.

- *step* 2, *Filtering:* The raw XBT and CTD data inevitably contain vertically small-scale geophysical and instrumental noise (e.g. spikes). Therefore, before applying the actual detection procedures, two filters are applied to the raw data (Rual, 1989): *i)* a non-linear Median filter known to eliminate completely the spikes in a signal, *ii)* a low-pass linear cosine Harming filter to smooth out the small scale noise.

In the present analysis, a 7-point Median filter without threshold logic is adopted. This filter can eliminate the spikes which consist of up to 3 data points (width of 2m; see Sy, 1985; or Brock, 1986, for details). After application of the Median filter, a simple 3-point Harming filter, with weights of 1/4, 1/2, 1/4, is applied 9 times, equivalent to a more sophisticated 11 -point Harming filter applied once. As a result, small-scale undulations with wavelengths less than about 5m are also eliminated with a minimum of transfer to longer wavelengths (see Blackman and Tukey, 1958, for details).

- *step 3, Calculation of temperature gradient:* Temperature gradients (hereafter TG) are calculated every metre from both filtered CTD and XBT data.

- *step 4, Detection of actual depth.* Reference XBT depths are defined at fixed XBT-depth intervals (i.e. at fixed elapsed times from the surface). For each of these reference XBT depths a fixed length depth-window defines a segment on the XBT temperature gradient (XBT-TG) profile. A corresponding depth-window, initially centred on the same depth, is shifted up and down along the CTD-TG profile until the area between the CTD and XBT segments of the temperature gradient profiles is minimised (see Fig. 3). The central depth of the shifted CTD segment, which gives the minimum value of the area, can be regarded as the acual depth of the reference XBT central point. The depth-shift of the CTD segment is the corresponding depth-correction. Therefore the elapsed time of the reference XBT central point can then be paired with its actual CTD depth to provide the corrected XBT depth-time data necessary for the calculation of the fall-rate equation in the next step.

In the present analysis, the depth-window is 50m wide, and its shifting range is from 30m above the central depth to 50m below it, by 1m steps. The estimates of the XBT actual depths are made at 25m intervals from 100m to the maximum depth (z_M). At less than 10Om, the temperature gradient is often very constant, or rapidly varying with internal waves leading to too many errors in the estimation. Thus, n_M, the maximum possible number of depth-time pairs (or of depth-differences) determined for a given profile is:

$$n_M = 1 + (z_M - 100) / 25 \tag{3}$$

This procedure can be automated, but a visual quality control of the depth-difference profiles is required in order to eliminate non-coherent depth-differences due to problems in the temperature profiles themselves.

3.1.2 *Procedures for the calculation of the depth-time equation coefficients*

- *step 5, Estimation of individual depth-time equations:* After the visual elimination of the non-coherent depth-differences and of their corresponding depth-time pair, the individual a_i and b_i coefficients for each profile are then determined by the method of least squares from the remaining corrected depth-time pairs:

$$z_i = a_i t - b_i t^2 \tag{4}$$

In the present analysis, coefficients calculated for profiles with less than 2/3 of n_M (3) have been eliminated. This elimination of the a_i and b_i calculated from an inadequate number of depth-time pairs is necessary to ensure the accuracy of the individual coefficients by providing a sufficient depth range, especially important for the *b* coefficient which characterises the curvature of the profile.

- *step 6, Estimation of the new depth-time equation:* Using the coefficients a_i and b_i from the profiles with a sufficient number of 'good' depth-time pairs, the mean coefficients, *A* and *B,* are calculated:

$$Z = At - Bt^2 \qquad \text{where } A = \text{mean } (a_i), \qquad B = \text{mean } (b_i) \tag{5}$$

7

3.1.3 *Remarks on the present method*

In Hanawa and Yoritaka (1987) and Hanawa and Yoshikawa (1991), temperature gradient extrema have been chosen as markers to detect depth-differences. In that case, it is relatively difficult to evenly distribute the data points from the surface to the bottom of the profile. This is because the existence of the extrema completely depends on the characteristic shapes of the temperature profiles. On the other hand, the present method can be applied to any temperature profile irrespective of the existence of extrema, and the data points are evenly distributed over the whole depth range. The only restriction is that the vertical temperature gradient must not be constant but has to change, at least slightly, within the search range of *step 4,* in order to allow determination of a depth-shift minimizing the area between the XBT and CTD temperature gradient profiles.

In Hanawa and Yasuda (1992), after the depth-error detection in *step 4,* there was an additional step to recalculate the XBT time matching a given true XBT depth. In addition, three more steps and an iteration were necessary after the calculation of the *tentative* revised equation before the determination of the *final* equation. The main difference between their method and our method is that their revised equations were calculated by a least square fit to the whole set of depth-time pairs calculated from all the profiles. They did not take into account the fact that all the depth-time pairs of a given profile are related by a relationship expressed by a depth-time equation specific of the profile (or by the coefficients a_i and b_i).

Another advantage of the present method is the easy addition of new data sets to a previous estimate of the mean A and B coefficients. Since the coefficients of (5) are the mean of all the individual coefficients, to add a new data set is simply to calculate the mean coefficients of the new data set *(steps 1 to 5)* and to take the weighted mean of the two estimates.

Thus this newly adopted method is simpler and more accurate than the previous method. It is more automatic, and demands only visual inspection of the depth-difference profiles to flag the depth-time pairs *(step 4).* However, the new method does also occasionally fail to detect depth-differences when the temperature gradient is constant in a section of the profile, or when the XBT temperature profile has features not matched by the CTD profile.

3.2 Depth-error distribution on the plane of the *a* and *b* coefficients

3.2.1 *The a-b plane: maximum depth-error isolines*

As shown in Hanawa and Yasuda (1992), it is possible to determine for a given depth range (depending upon the probe type) the maximum absolute depth-difference between a reference depth-time equation (coefficients *A* and *B)* and any other depth-time equation (coefficients *a* and *b).* As fully described in Appendix 1, this maximum depth-error is not always located at the same depth, hence a maximum relative depth-error may be a better representation. However, this relative error can be maximum at the surface, where the absolute depth-error is zero. The best representation may therefore be the maximum absolute depth-error expressed as a relative depth-error (i.e. divided by its depth).

Isolines of all these depth-errors can be calculated and plotted on a plane defined by the *a* and *b* coefficients of all the depth-time equations (called hereafter the *a-b* plane). Examples of such plots, and how to calculate them, are given in Appendix 1. Two lines related to these isolines, the transfer line and the discontinuity line (which are defined in the same appendix), divide the *a-b* plane into four sectors where the maximum depth-error differs by its type or its depth and sign. In two of the sectors (upper-left and lower-right) the depth of the maximum error is constant, whilst in the other two sectors it is variable within a certain depth-range. The only zero-error point on the *a-b* plane is the reference *AB* point. Along the discontinuity line the variation of the depth-error is at a minimum, due to the fact that the depth-error curve is more or less symmetrical about the zero-error axis (Fig. A 1.1, curve 4).
Therefore the isolines define a central area, elongated along the discontinuity line, where the maximum depth-error is small even when the *a* and *b* coefficients are largely different from those of the reference equation. Hence, if the coefficients of individual profiles or individual data subsets are distributed within this depth-error region, the error may be within the instrumental noise and a unique depth-time equation can be computed.

8

Thus, by using the *a-b* plane, one can: *i) see* at a glance whether or not an *ab* point is within the manufacturer's specification, *ii)* determine its maximum depth-error, *iii)* depending upon the sector, determine the error type and the depth of the maximum error.

3.2.2 *Statistics on the a-b plane*

The individual *ab* points, calculated in *step 5,* can be considered as samples of two correlated quasi-normal variables (see again Appendix 1). The confidence interval of such a bi-variate normal distribution is represented by an ellipse centred on the mean *AB* point (Fig. Al .5), and its equation is a function of the correlation coefficient *r* between *a* and *b* and of the standard deviations of each variable. In order to know the confidence level of the area enclosed by an ellipse of *n* standard deviations, one must refer to tables of the cumulative bi-variate normal density function (i.e. Owen, 1962) however, if n and *r* are high enough, the confidence levels are close to those of a single normal variable. Hereafter these ellipses will be called the 'individual' statistical ellipses.

The statistical distribution and the confidence interval of the mean *AB* point can moreover be represented by a 'mean' statistical ellipse (using the standard error of the mean). It has the same confidence level as the 'individual' ellipse, and its axes have the same directions as the axes of the corresponding 'individual' ellipse, but they are divided by the square-root of the number of points used to calculate that mean. The 'mean' ellipse is, in fact, the probable area where the actual mean lies, so it can be considered as the actual 'size' of the calculated mean point.

4. New Depth-Time Equation for T-7 XBTs

4.1 Quality control of the data

Mechanical application of the detection procedures described in the previous subsection will be adequate only for ideal XBT/CTD comparison data. Actual XBT data sometimes include imperfections due to problems such as bowing and wire stretching (see Bailey *et al.,* 1989 and 1994; Sy 1991). In addition, temperature profiles themselves are sometimes inappropriate for comparison, especially if there are no change at all in the temperature gradients such as those associated with some very well mixed isothermal layers, etc. Therefore, an inspection of the comparison data for imperfections is required. In this subsection, examples will be shown to demonstrate the effect of such problems on the procedures.

Figure 4 shows three typical examples of XBT/CTD comparisons: 07A16, C7B08 and T7A03. Generally, the temperature gradient profiles of the CTD and XBT correspond well to each other, for example 07A16. On the other hand, C7B08 is an example obviously affected by a bias-like temperature error, but the temperature gradient profiles of the XBT and CTD nevertheless correspond well to each other. Example T7A03 not only includes a bias-like temperature error, but is probably also influenced by wire stretching and/or wire insulation penetration type defects, most obvious around 600m. Therefore, the XBT temperature gradient profile does not correspond well to that of the CTD data, especially below 350m. The XBT depth-error profile of07A16 is seen to be monotonically increasing from -2m at 100m to -22m at 750m, whilst C7B08 is almost monotonically increasing from -lm at 10Om to -22m at 700m. This example shows that, as already mentioned, this method can reasonably detect the depth-difference even for XBT data having bias-like temperature errors. On the other hand, although T7A03 shows a plausible profile from 100m to 350m, it largely deviates and scatters in the depth-error profile from 400m downward. In this case, such non-coherent deviations in the depth-difference data (marked by stars in the figures) are manually discarded at the end of *step 4* before the estimation of the individual equation in *step* 5.
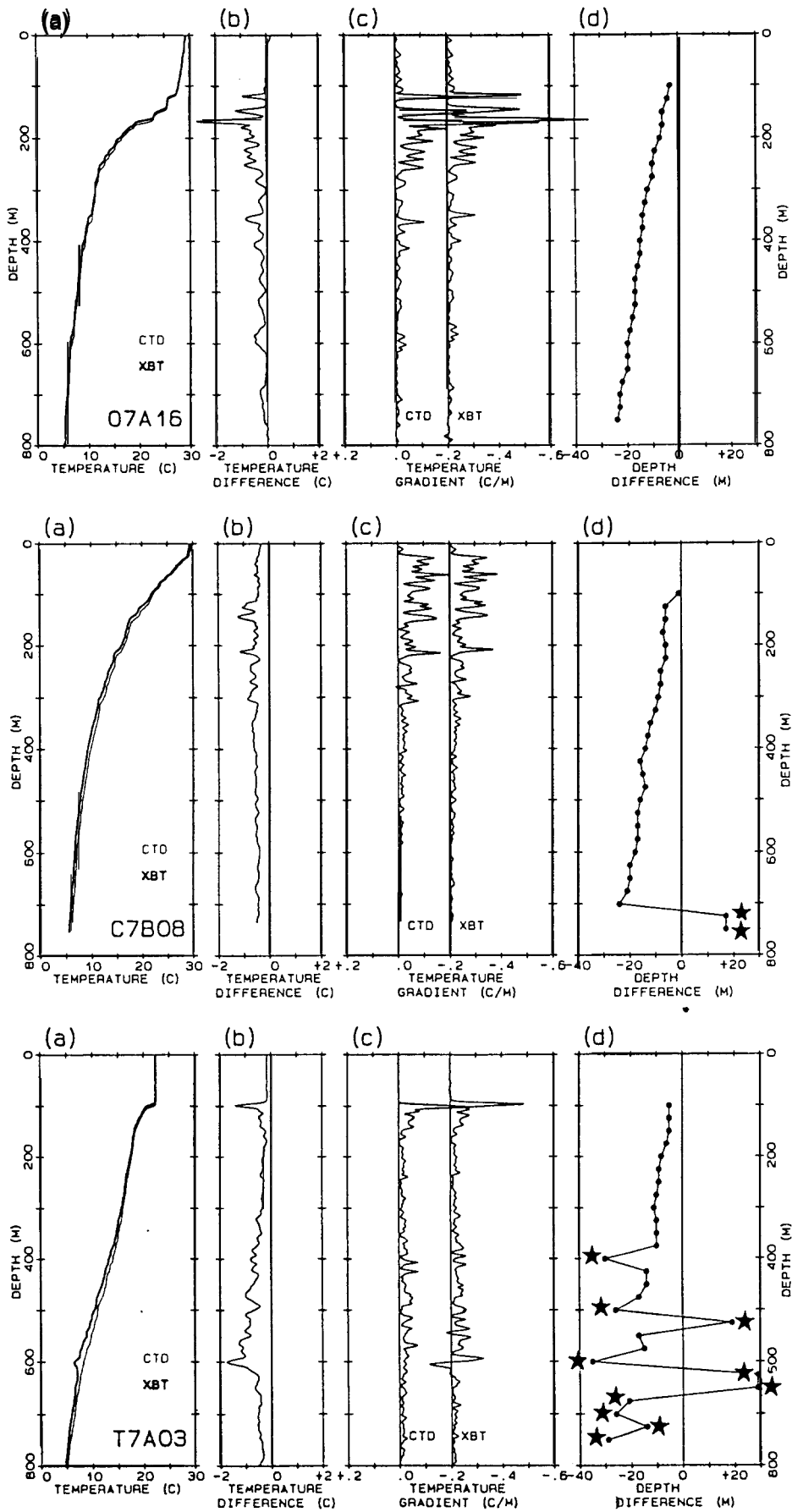
Figure 4. Three typical examples of comparison data: 07A16, C7B08 and T7A03 (see Table 1 for details): (a) CTD (thin line) and XBT (thick line) temperature profiles; (b) profile of the temperature difference (XBT minus CTD); (c) CTD and XBT temperature gradient profiles (XBT temperature gradient profiles are offset by -0.2°C/m); (d) detected XBT depth-errors. Depth-errors marked by * are considered erroneous and discarded.

10

In addition to the examples shown in Fig. 4, the detection of the depth-error sometimes failed when tile surface mixed layer was deeper than 100m. In such a case, the depth-difference data are also manually discarded after a visual inspection of the depth-difference profile. Due to the overall coherence of the depth-error profile, it is in general not difficult to determine which depth-difference data should be discarded from, or included in the analysis.

4.2 Calculation of the new depth-time equation for T-7 XBTs

The Sippican-TSK depth-time equation for T-7 XBTs (and for T-4/T-6 XBTs) is:

$$z_{\mathrm{m}} = 6.472t - 0.00216t^2 \qquad (6)$$

By using the detection method described, the depth-difference data were estimated for 161 T-7 XBT profiles (see Table *la*). After examination of the depth-difference profiles, five of the T-7 XBTs were completely discarded from the analysis due to a general mismatch between the CTD and XBT profiles as a result of XBT malfunctions, etc.

The depth-time equations were calculated *(step 5)* for each individual T-7 profile, and the A_7 and B_7 coefficients of the new depth-time equation obtained *(step 6)* by calculating the mean of the individual a_i, b_i coefficients belonging to the 'good' profiles (profiles with 18 to 27 'good' depth-differences, i.e. profiles with a minimum of 2/3 of n_M, the maximum number of depth-differences calculated for T-7 probes, see (3) in *step* 3). Out of 156 individual a_i, b_i coefficients, 125 met that criterion. The new depth-time equation for the T-7 probes is estimated as:

$$Z_7 = 6.701\,t - 0.00238t^2 \qquad (7)$$

As *a* and *b* were found to be quasi-normally distributed variables, their standard deviations can be calculated (see Table la). The confidence intervals for the individual a_i and b_i and for the mean A_7 and B_7 coefficients, at a confidence level of 95°/0, are:

$$
\begin{aligned}
a_7 &= 6.701 \pm 0.260 & b_7 &= 0.00238 \pm 0.00182 \\
A_7 &= 6.701 \pm 0.023 & B_7 &= 0.00238 \pm 0.00016
\end{aligned}
$$

4.3 T-7 probes on the *a-b* plane

The T-7 *a-b* plane, centred on the reference AB_7 point (see equation 7), is presented in Fig. 5 for a maximum depth of 800m. Even though the manufacturers' rated depth is 760m for the T-7 probe, the T-7 probe's actual maximum depth is very often over 800m (compared to the actual CTD depth). The cloud of the 125 individual T-7 *ab* points used to calculate the coefficients of (7) are also shown. As the *a* and *b* can be considered as correlated bi-variate quasi-normal variables with a correlation coefficient of 0.85, the 'individual' 1, 2, 3 standard deviation ellipses (see Appendix 1) have confidence levels close to 58°A (and not 68% as for an independent variable), 95% and 99.7% respectively. One can see that the 'individual' 1-standard deviation ellipse is close to the ±5m isoline, and the 'individual' 2-standard deviation ellipse is within the ±2% isoline, so the maximum depth-error for the T-7 probes is not very far from the manufacturers' specifications when using the new equation (7) (the manufacturers' specifications are ±5m or ±2% of the depth, whichever is the greatest). But this is not true for the depth-error at all depths, as will be demonstrated later. The 'size' of the mean AB_7 point with a confidence level of 95°/0 is given by the small two standard-error-of-the-mean ellipse.

The ab_m point of the manufacturers' equation is well outside the cloud of observed *ab* points, at 3 'individual' standard deviations from the reference AB_7 point, in a sector where the maximum depth-error is: -25m (from equation Al.8 in Appendix 1) or -3. 15% (A 1.27) at a depth of 800m.
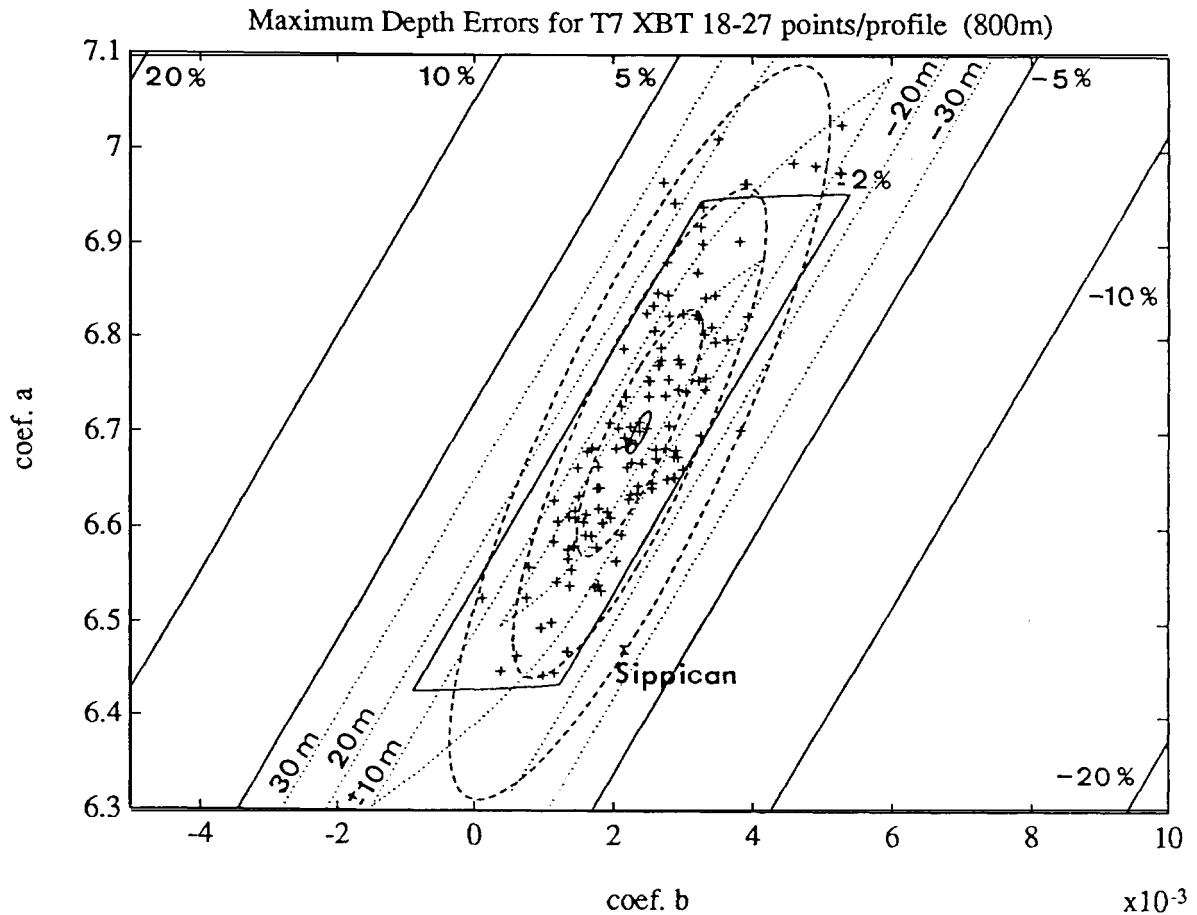
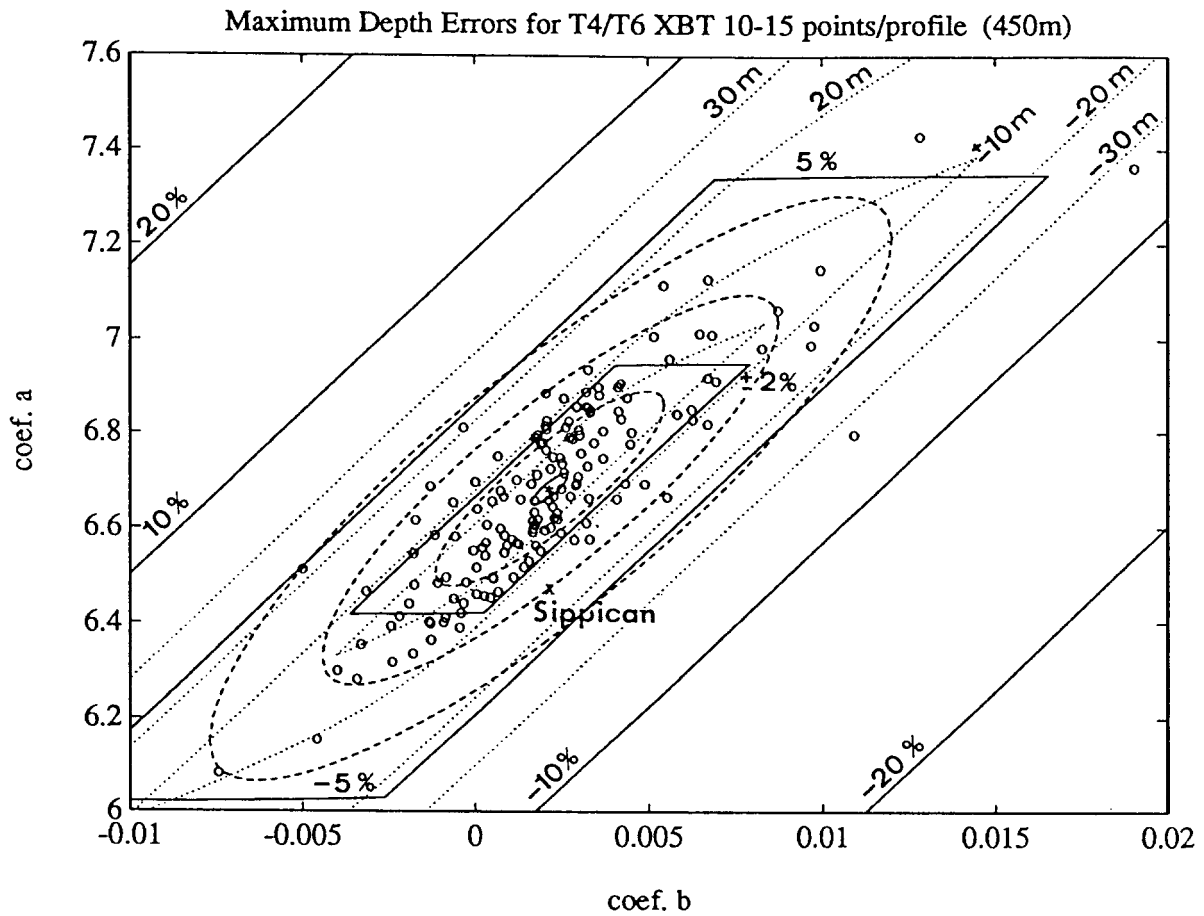Figure 5, T-7 XBT probes on the a-b plane of the new T-7 equation (Eq. 7, reference AB_7 point marked by an * at the center of the ellipses: $A_7 = 6.701$, $B_7 = 0.00238$, see Appendix 1 and Table 1 for full explanations):

i) The crosses are the 125 individual T-7 *ab* points used to calculate the coefficients of new equation (7).

ii) The maximum absolute depth-error isolines (dotted lines) are calculated down to 800m (±5m is not labelled for clarity). The solid lines represent the same error expressed in percentage of its depth. Along the discontinuity line of the dotted isolines (not drawn, see Fig. Al .2), the depth of the *first derivative* error is 278m. It is 340m along the discontinuity line of the solid isolines (not drawn, see Fig. A 1.4).

iii) The dashed ellipses are the individual 1, 2, 3 standard deviation ellipses, their confidence levels are, respectively, 58% (and not 68%), 95% and 99.7%. The small central solid line ellipse is the 2 standard-error-of the-mean ellipse of the mean AB_7 point. See Table 1 *a* for details.

iv) The manufacturer's equation ab_m point is marked by an *X* (Sippican). Its maximum depth-error is the *deepest* error: -25m or -3. 15% at the depth of 800m.

Figure 6.   T-4/T-6 XBT probes on the *a-b* plane of the new T-4/T-6 equation (Eq. 8, reference AB_{46} point marked by an * at the center of the ellipses: $A_{46} = 6.683$, $B_{46} = 0.00215$), (the scales of that figure are twice the scales of Fig. 5, therefore the area shown is 4 times greater):

    i) The circles are the 160 individual T-4/T-6 *ab* points used to calculate the coefficients of the new equation. (8).

    ii) The maximum absolute depth-error isolines down to 450m are equivalent to those in Fig. 5. Along the discontinuity lines the depth of the *first* derivative error is 153m (dotted isolines), or 189m (solid isolines).

    iii) The ellipses have the same meaning as in Fig. 5 (see Table 1 *b* for details).

    iv) The maximum depth-error of the manufacturer's ab_m point *(X)* is the *deepest* error: - 15m or 3.24% at the depth of 450m.

T4/T6, T7 XBT, Mean AB points & stat. ellipses

(figure: Standard deviation ellipses on the a-b plane; y-axis "coef. a" from 6.3 to 7.1; x-axis "coef. b" from 0 to 5 ×10⁻³; curves labelled T7, T46, 2 S T46, 2 S T7)

Figure 7 Standard deviation ellipses on the *a-b* plane of the T-4/T-6 and T-7 mean *A, B* coefficients (the *b* scale is 3 times smaller than in Fig. 5): i) The outside dashed ellipses and the large solid ellipse are respectively the T-4/T-6 and T-7 'individual' 2-standard deviation ellipses of Figs. 5 and 6. ii) The small intersecting dashed and solid ellipses are the 1, 2, 3 standard-error-of-the-mean ellipses for, respectively, the T-4/T-6 and the T-7 *ab* points.

Table 2 Summary by region, or manufacturer, of the CTD-XBT comparison experiments for the combined data set of T-4/T-6/T-7 XBTs. Field areas are shown on Fig. 1. Same columns as in Table 1 except that the individual data sets have been grouped together, and that column 4 of Table 1 has been removed.

Regional & Manufacturer's Data sets	Number of Profiles	'Good' Profiles 2/3n_M	Probe Types & Manuf.	Field Experiments Date	Field Experiments Institution	XBT recorder	CTD profiler	A	B 10⁻⁵	Max. Depth-error metre	Max. Depth-error %	Correl. coef. (AB)	σ_A 10⁻³	σ_B 10⁻⁵	σ_a 10⁻³	σ_b 10⁻⁵
				Manufacturers' Equation (6) :				*6.472*	*216*	*-25.9*	*-3.24*					
NW Pac. (*nwp*, 1)	54	50	T67 Tsk	1985-87-89 1991-92	TOHOKU	ORI Z-60-II	NB IIIb	6.669	223	-2.4	-0.30	0.87	22	22	154	154
NW Trop.Pac. (*nwtp*, 2)	9	9	T7 Tsk	1987	TOHOKU	ORI	NB IIIb	6.652	201	-1.6	-0.30	0.78	20	27	61	81
W Equat.Pac. (*wep*, 4)	101	70	T47 Si.	1989-91-92	ORSTOM	Argos	SBE-9	6.662	201	-0.9	-0.22	0.89	26	46	221	388
SW Trop.Pac. (*swtp*, 5)	76	57	T467 Si.	1989-91-92	ORSTOM	Argos	SBE-9	6.694	249	-3.4	-0.42	0.84	23	37	170	280
Tasman Sea (6)	12	6	T7 Si.	1989	CSIRO	Mk-9	NB	6.747	200	10.9	1.36	0.84	69	38	169	93
SE Indian (*sei*, 3)	21	13	T7 Si.	1987	CSIRO	Mk-9 SA-810	NB	6.666	224	-3.0	-0.37	0.94	29	19	105	68
Bahamas (7)	21	15	T4 Si.	1992	NOAA/NOS	Mk-9	NB III	6.514	061	-4.8	-1.35	0.93	32	53	123	205
NW Trop.Atl. (*nwta*, 8)	66	55	T467 Si.	1988-91	NOAA/NOS SIPPICAN	Mk-9 Argos	NB III	6.822	293	6.3	1.00	0.73	11	16	85	119
NE Atlant. (*nea*, 9)	12	10	T7 Si.	1991	BSH	Mk-12	NB III	6.561	179	-9.1	-1.13	0.92	34	30	108	93
T7 Sippican	115	83	Sippican	1987 to 92				6.698	235	-0.7	-0.09	0.82	14	10	131	87
T4/T6 Sippican	194	143	Sippican	1988 to 92				6.697	221	0.6	0.13	0.86	18	28	210	340
T7 TSK	46	42	TSK	1985 to 91				6.707	242	-0.7	-0.12	0.91	20	15	129	100
T6 TSK	17	17	TSK	1989 - 92				6.566	164	-5.7	-1.27	0.97	31	52	129	213
T4/T6 Global	211	160		new T4/T6 equation (7) :				6.683	215	-0.2	-0.06	0.86	16	26	206	329
T7 Global	161	125		new T7 equation (8) :				6.701	238	-0.8	-0.10	0.85	12	8	130	91
T4/T6/T7	372	285		New T4/T6/T7 Equation (9) :				6.691	225	-	-	0.83	10	15	177	254

14

5. New Depth-Time Equation for T-4 and T-6 XBTs

By applying the same procedures used for estimating the new depth-time equation for the T-7 XBT data, the new depth-time equation for the combined T-4 and T-6 XBT data (160 profiles with 10 to 15 good depth-differences; i.e. those profiles with a minimum of 2/3 of the maximum number of depth-differences for T-4/T-6 probes), is estimated as:

$$Z_{46} = 6.683 \, t - 0.00215 \, t^2 \tag{8}$$

As a and b were also found to be quasi-normally distributed variables, their standard deviations can also be calculated (see Table 1 b). The confidence intervals for the individual a_i and b_i and for the mean A_{46} and B_{46} coefficients, at a confidence level of 95%, are:

$$a_{46} = 6.683 \pm 0.412 \qquad b_{46} = 0.00215 \pm 0.00658$$
$$A_{46} = 6.683 \pm 0.033 \qquad B_{46} = 0.00215 \pm 0.00052$$

5.1 T-4/T-6 probes on the *a-b* plane

Figure 6 shows the cloud of the 160 individual T-4/T-6 *ab* points used to calculate the coefficients of (8). The T-4/T-6 XBTs actual maximum depth is very close to the manufacturers' rated depth of 460m, so 450m will be considered as the maximum T-4/T-6 depth. The ellipses in Fig. 6 are 1, 2, 3 standard deviation ellipses for the individual $a_i b_i$ points (see Appendix 1) which, with a correlation coefficient of 0.83, correspond to 57°/0, 95°/0 and 99.7°/0 confidence levels respectively. In addition, the small two standard-error-of-the-mean ellipse has been included to show the 'size' of the mean AB_{46} point. As for the T-7 probes, the 'individual' one standard deviation ellipse is close to the ±5m isoline. The 'individual' 2-standard deviation ellipse, however, is just outside the ± 2% isoline. There is a far greater scatter of the individual *ab* points for the T-4/T-6 profiles than for the T-7 profiles (note the different axes scales on Figs. 5 and 6). This is particularly the case for the individual b_i points. This was found in part to be due to the shorter maximum depth available for the least squares calculation in *step* 5, but is mainly due to the greater probe-to-probe fall rate variability of the T-4/T-6 probes.

The manufacturers' equation ab_m point in Fig. 6 is again outside the main cloud of observed *ab* points, at 2 'individual' standard deviations from the reference point, in a sector where the maximum depth-error is the *deepest* error; -15m (Al .8) or -3.24% (Al .27) at the depth of 450m.

5.2 Comparison with the New T-7 Depth.Time Equation

If one examines, on the same *a-b* plane, the two series of statistical ellipses for the 160 T-4/T-6 *ab* points and the 125 T-7 *ab* points respectively (Fig. 7), one can see that: *i)* The T-7 'individual' two-standard deviation ellipse is completely embedded in the T-4/T-6 'individual' two-standard deviation ellipse. *ii)* The T-7 one, two, and three standard-error-of-the-mean ellipses intersect with the corresponding T-4/T-6 'mean' ellipses. Therefore, the T-7 and T-4/T-6 populations and their means are not significantly different from a statistical point of view and we can safely determine a new equation for the combined T-4/T-6/T-7 XBT data set.

6. New Reference Depth-Time Equation for T-7, T-6, and T-4 XBTs

Before mixing together the T-7 and the T-4/T-6 *ab* data sets the normality of the distributions of the coefficients has to be verified in order to iustify the calculation of a mean and its statistics. The distributions were found to be quasi-normal (skewness coefficients of 0.3 and 1.2, and kurtosis coefficients of 1.6 and 9.0 for the a_i and b_i coefficients respectively). The large tails in the b_i coefficient distribution are indicative of the previously discussed scatter of the b_i coefficients on the *a-b* plane, especially for the T-4/T-6 probes.
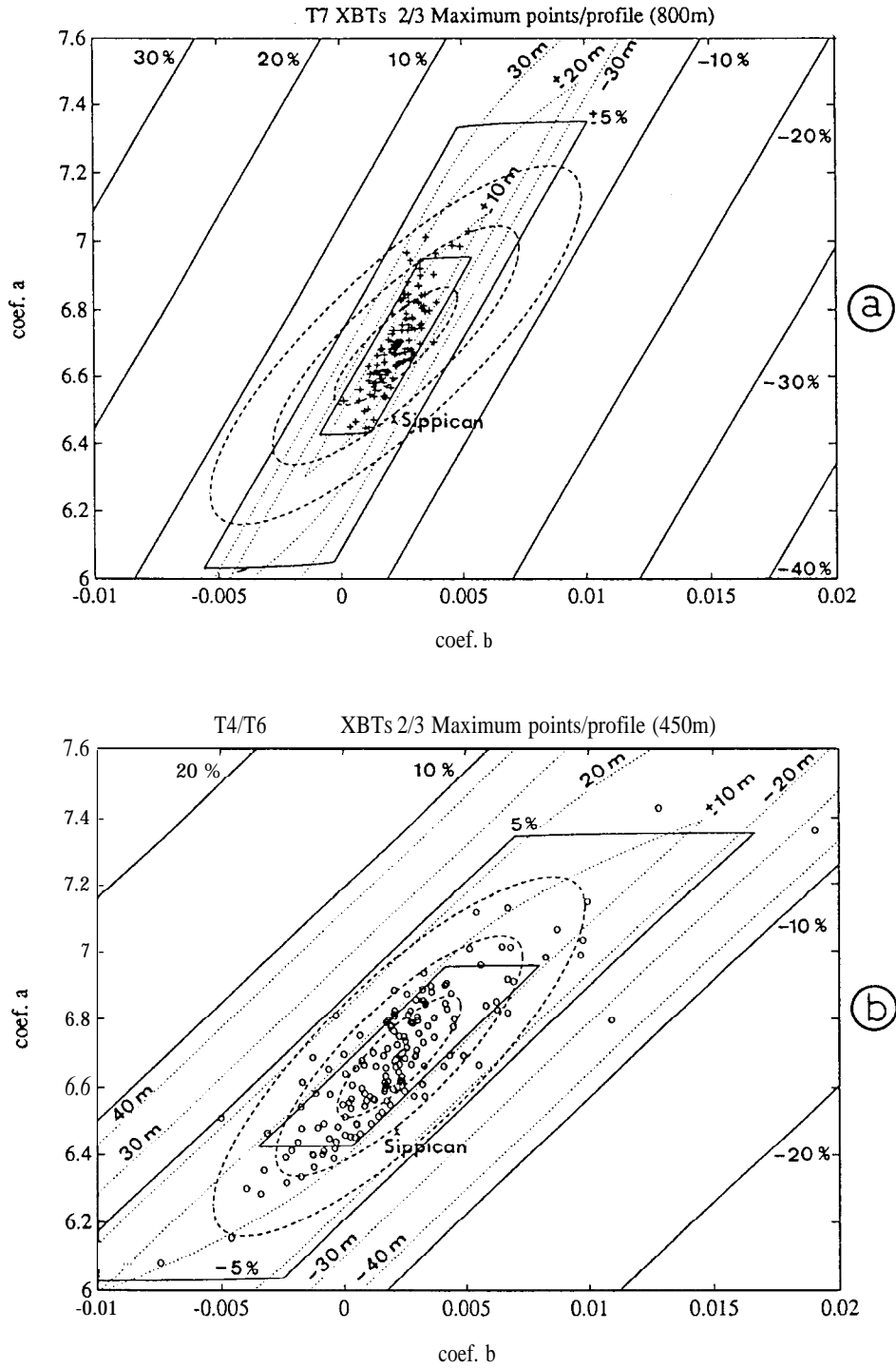
15

Figure 8.   T-7 (upper) and T-4/T-6 (lower) data sets presented on their respective *a-b* plane of the new T-4/T-6/T-7 equation (800m or 450m maximum depth; same scales as Fig. 6).   The reference $A\,B_{467}$ point $(\,A_{467} =$ 6.691, $B_{467} = 0.00225$; marked by an *) is at the center of the ellipses.

   i) The maximum absolute depth-error isolines are equivalent to those in Figs. 5 and 6. Along the discontinuity line of the maximum absolute depth-error the depth of the first *derivative* error is 340m on the T-7 *a-b* plane, and 189m on the T-4/T-6 *a-b* plane. It is, respectively, 277m or 153m for the same depth-error but expressed as a relative error.

   ii) The dashed ellipses and the small solid ellipse have the same meaning as in Fig. 5 (see Table 2 for details).

   iii) The maximum depth-error of the manufacturer's ab_m point *(X)* is the *deepest* error: -26m or -3.24% at the depth of 800m, and -15m or -3.26% at the depth of 450m.

16

After calculating (step 6) the mean A_{467} and B_{467} coefficients from the combined T-7 and T-4/T-6 data set (see Table 2), the new reference depth-time equation is given by:

$$Z_{467} = 6.691 \; t \; - \; 0.00225 \; t^2 \tag{9}$$

The confidence intervals for the individual a_i and b_i and for the mean A_{467} and B_{467} coefficients, at a confidence level of 95%, are:

$$a_{467} \; = 6.691 \pm 0.354 \qquad\qquad b_{467} = 0.00225 \pm 0.00508$$
$$A_{467} = 6.691 \pm 0.021 \qquad\qquad B_{467} = 0.00225 \pm 0.00030$$

The normalised standard deviations of the mean, σ_A / A and σ_B / B are, respective>, equal to 0.16% and 6.7%. The quadratic term B being a corrective second order term it is normal, for it, to be less accurately determined, specially when adding shallow probes such as the T-4/T-6 probes.

6.1 T-4/T-6/T-7 probes on the *a-b* plane

Depending on which type of probe is to be evaluated for depth-errors on the *a-b* plane, the results from the combined data set can be presented either on the T-7 *a-b* plane (800m maximum depth) or on the T-4/T-6 *a-b* plane (450m maximum depth), as shown in Figs. 8a and 8b respectively. The ellipses in Fig 8 are 'individual' 1, 2, 3 standard deviation ellipses for the $a_i b_i$ points (see Appendix 1) which, with a correlation coefficient of 0.83, correspond to confidence levels of 57%, 95% and 99.7% respectively. In addition, the small two standard-error-of-the-mean ellipse has been included to show the 'size' of the mean AB_{467} point.

In Fig. *8a*, the maximum depth-errors for the individual T-7 probes and the 'individual' one standard deviation ellipse for the AB_{467} reference point are mostly within the $+2°/0$ and ± 10 metres isolines, although some are outside the $+20$m isoline. On the T-4/T-6 *a-b* plane (Fig. 8b), the T-4/T-6 individual probes are more scattered, although the maximum depth-errors are still generally within in the 2% and ± 10 metre isolines, with several points just within the $\pm 5\%$ and ± 20 metre isolines.

The manufacturer's equation ab_m point is outside the main cloud of observed *ab* points in both Figs. 8a and 8b, at over 2 'individual' standard deviations from the AB_{467} reference point, in a sector where the maximum depth-error is the *deepest* error: -26m (A 1.8) and -3.24% (A 1.27) at the depth of 800m, or -15m and. -3.26% at 450m.

6.2 Comparison with the T-7 and the T-4/T-6 New Depth-Time Equations

The T-7 and T-4/T-6 mean *AB* points are within one standard-error-of-the-mean from the AB_{467} reference point (see Table 2). The maximum absolute depth-error between the AB_{467} reference point and the T-7 *AB* point is -0.8m or -0.1% at 800m (Al.8 and Al .27); between the AB_{467} reference point and the T-4/T-6 *AB* point it is -0.2m or -0.06% at 264m (Al .7, Al .26 and Al .6). These results confirm that a single reference T-4/T-6/T-7 depth-time equation can replace, with very reasonable accuracy, tile original manufacturers' equation.
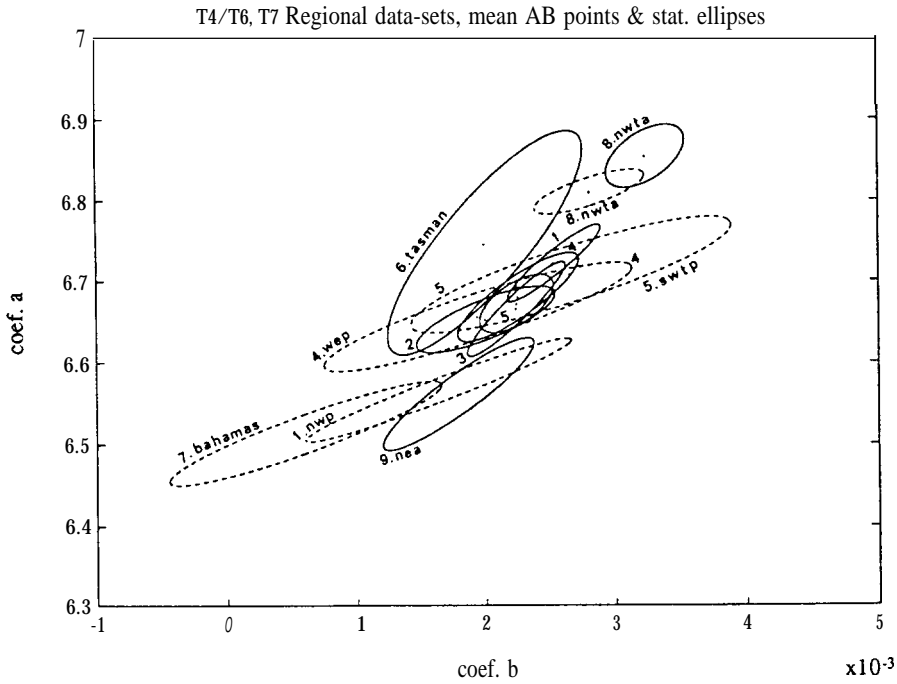
17

T4/T6, T7 Regional data-sets, mean AB points & stat. ellipses

Figure 9   Mean regional two-standard-error-of the-mean ellipses on the *a-b* plane(95% confidence level); see Fig. 1 and Table 1 for the location of the regions). The full and the dashed ellipses are, respectively, the T-7 and the T-4/T-6 mean regional ellipses. For clarity, in the medium group some ellipses are referred to by their region number only.
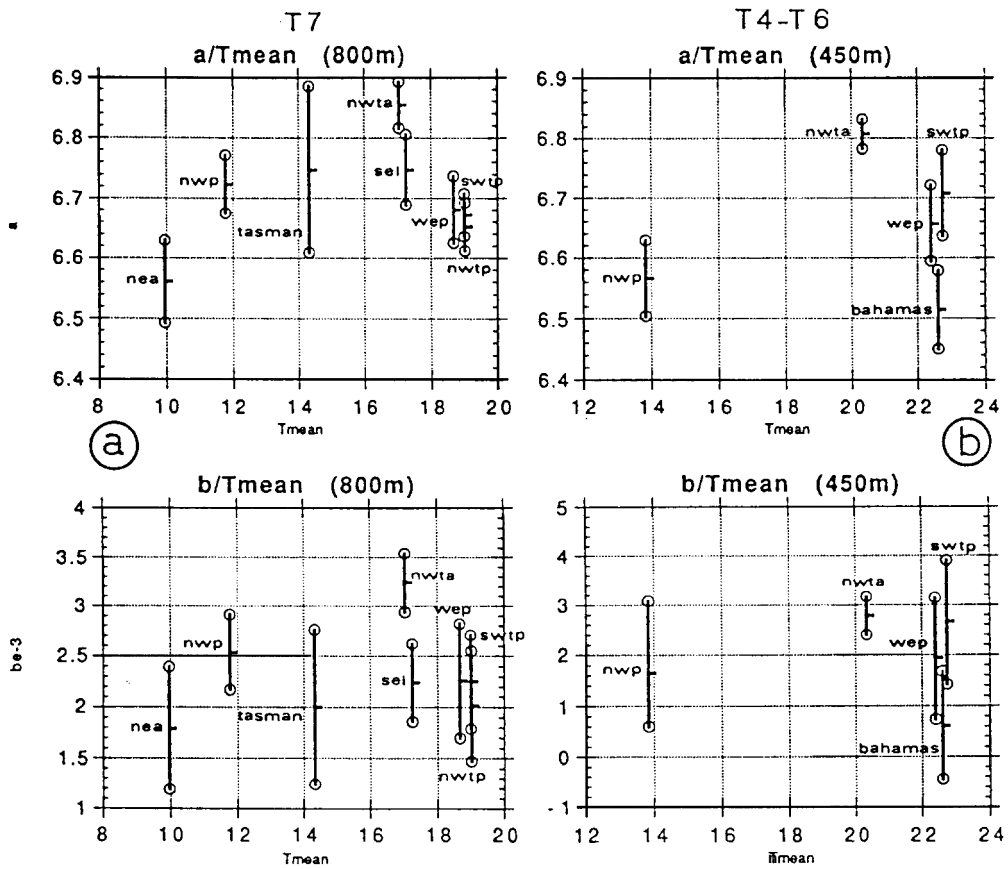

Figure 10   The mean *A, B* coefficients and the two-standard-error-of-the-mean bars for the different regions of the XBT-CTD experiment are plotted against the mean temperature of the water between the surface and the maximum depth reached by the probe type (a: 800m for T-7, b: 450m for T-4/T-6). See Fig. 1 for the location of the regions. The mean temperature has been computed using the Levitus (1982) T-S data of Fig. 2.

18

6.3 Inter-comparisons of the Individual Data Sets

6.3.1 *Regional comparisons*

Figure 9 shows, on the *a-b* plane, the two standard-error-of-the-mean ellipses (95%) of the mean *AB* points for each regional data set. These ellipses define 3 main significant groups whose domains do not intersect: *i)* A slow fall rate group, which includes the T-7 north-eastern Atlantic *(nea),* the T-4 Bahamas and the T-6 north-western Pacific *(nwp)* data sets; *ii)* A high fall rate group which includes the T-7 and the T-4/T-6 north-western tropical Atlantic data sets *(nwta); iii)* A medium fall rate group which includes all the other regional groups, except the T-7 Tasman data set. The ellipse for this data set, which has only 6 probes, is too wide to belong to one group. It is mainly an high fall rate data set, but it also covers part of the medium group.

The three groups appear to show no overall regional homogeneity. The slow fall rate group ranges from tropical latitudes to high latitudes in the northern hemisphere. The medium fall rate group is mainly a tropical and subtropical group, but includes the T-7 north-western Pacific data set which is a mid-latitude data set. The Tasman data set, which is also a mid-latitude data set, ranges from medium to high fall rates. The T-6 and T-7 north-western Pacific data sets are found in different groups, i.e. the slow and medium fall rate groups respectively.

Although there were no opportunities to collect data in extreme oceanic conditions, the data presented in this study were collected in several different regions in order to examine the possible influence of different water masses on the fall rates of the probes. One of the parameters for understanding the dynamics of a moving body in water is viscosity (Seaver and Kuleshov, 1982). Viscosity is, to the first order, inversely proportional to the temperature, therefore the mean temperature over the water column may be used to represent the mean viscosity. Another parameter is the density, but in our case, the correlation is very high (-0.91) between the mean density and the mean temperature, therefore the results found for the mean viscosity are applicable to the mean density. Figure 10 presents the mean regional *A* and *B* coefficients as a function of this mean temperature calculated between the surface and the maximum depth reached by the probe type (800m for T-7, 450m for T-4/T-6). The expected influence, if any, should be a decrease in the speed of the probes (decrease of *A* mainly) with increasing viscosity. The only significantly different pairs of *A* coefficients are: the north-western tropical Atlantic *(nwta),* a medium viscosity data set, and the north-eastern Atlantic *(nea),* an high viscosity data set, for the T7; and the same *mwta* and the north western Pacific *(nwp)* for the T-4/T-6 probes. For these two pairs of data sets the theoretical linear change in the fall rate is very close to the observed change of 0.3 m/s for the T-7 and 0.22 m/s for the T-4/T-6. But if other pairs of data sets are considered, an inverse relationship can be found (i.e. *nwp and nwtp* for the T7, or *nwp* and *bahamas* for the T-4/T-6). This may be due to the variability of the probe shape, and/or weight, generating different turbulent drags, completely obscuring the viscosity influence. In fact, considering all the regional data sets, it is very difficult to find a global relationship and most of the regional *A* and *B* coefficients are not significantly different at a 95% confidence level.

6.3.2 *Onboard equipment comparisons*

The data sets in the medium fall rate group of Fig. 9 were collected by almost all of the different types of onboard XBT and CTD equipment used in the study (see Table 1). Therefore, no significant influence of the type of onboard-system on the fall rate appears to exist.

Moreover, in the north-western tropical Atlantic *(mwta),* in the north-western Pacific *(nwp)* and in the south-eastern Indian Ocean *(sei),* respectively, comparisons were made using, in the same area, the same type of XBT but different onboard systems (see Table 1). No significant differences were observed in the fall rates for the *nwta* or for the *nwp* data sets, when the data were grouped by onboard equipment. The two standard-error-of-the-mean ellipses are almost tangent for the *sei* case (not shown), but the two mean *AB* points are so close that the induced error is small (5m at 800m or 0.6%).
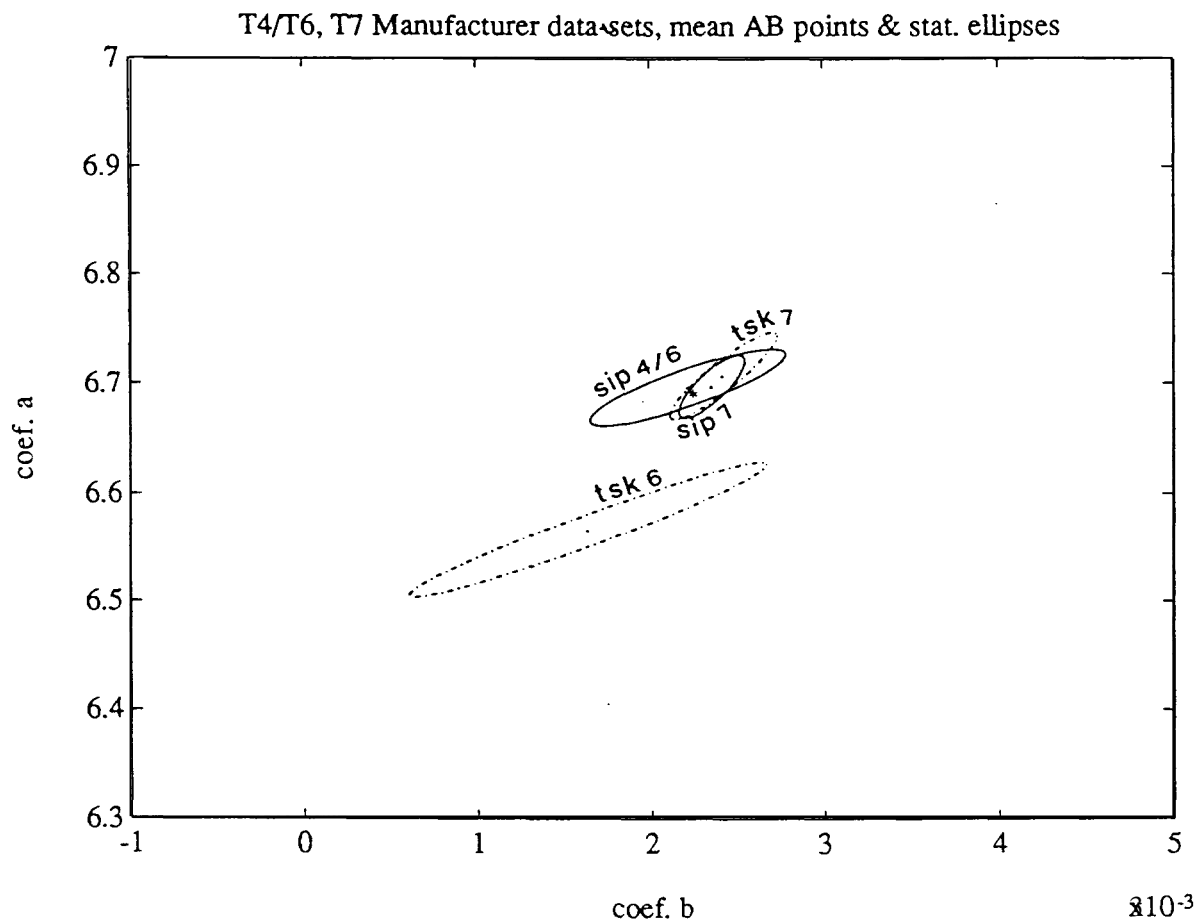
19

Figure 11   Mean Sippican and TSK T-7 and T-4/T-6 *AB* points and their two-standard-error-of-the-mean ellipses on the *a-b* plane (95% confidence level; same scale as Fig. 9; see Table 2 for detailed information).
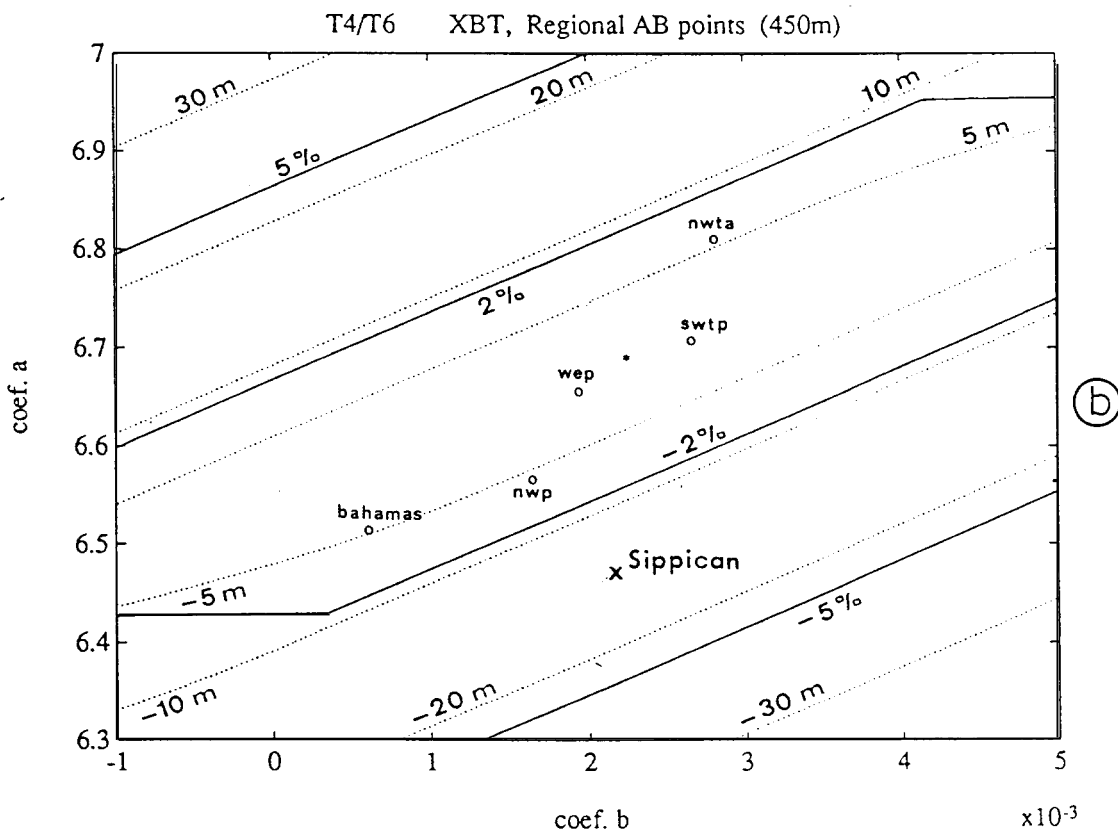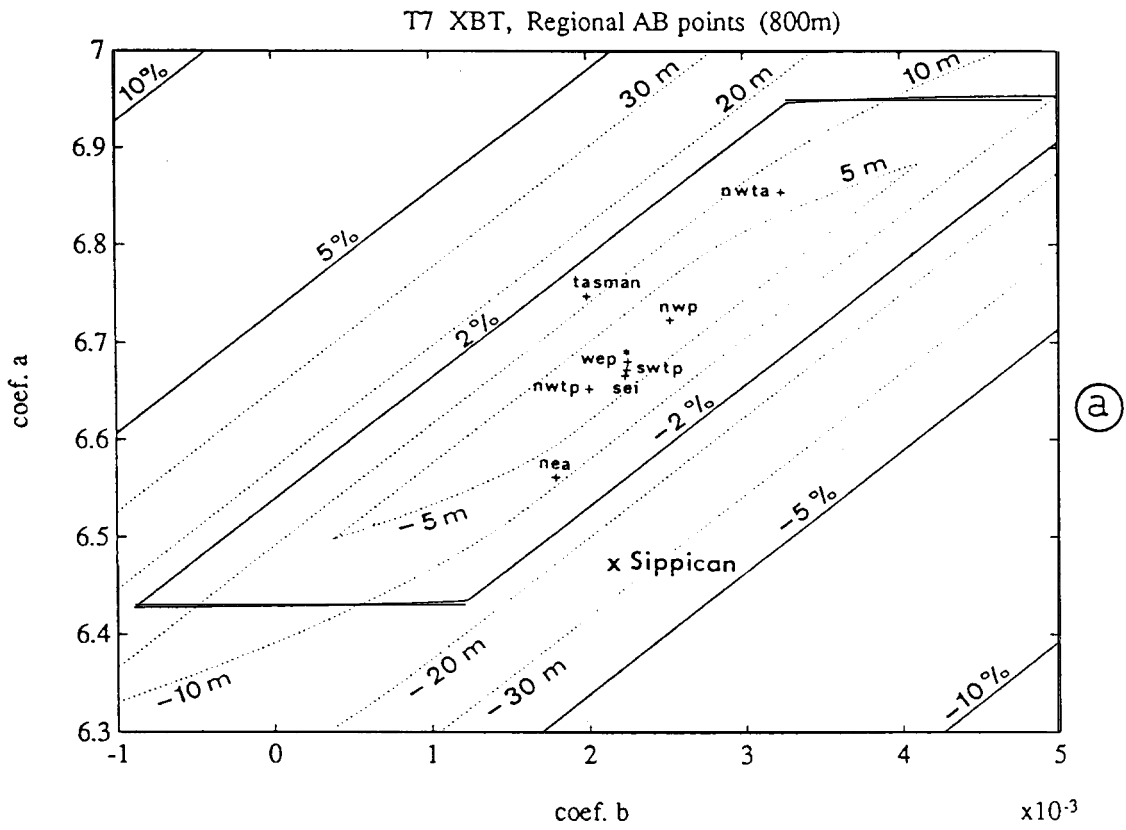
T7 XBT, Regional AB points (800m)

T4/T6 XBT, Regional AB points (450m)

Figure 12   Regional AB points on the new AB_{467} (marked by an *) reference planes of Fig. 8 (T-7 800m and T-4/T-6 450m maximum depth-error planes), but with the scales of Figs. 9 and 11.
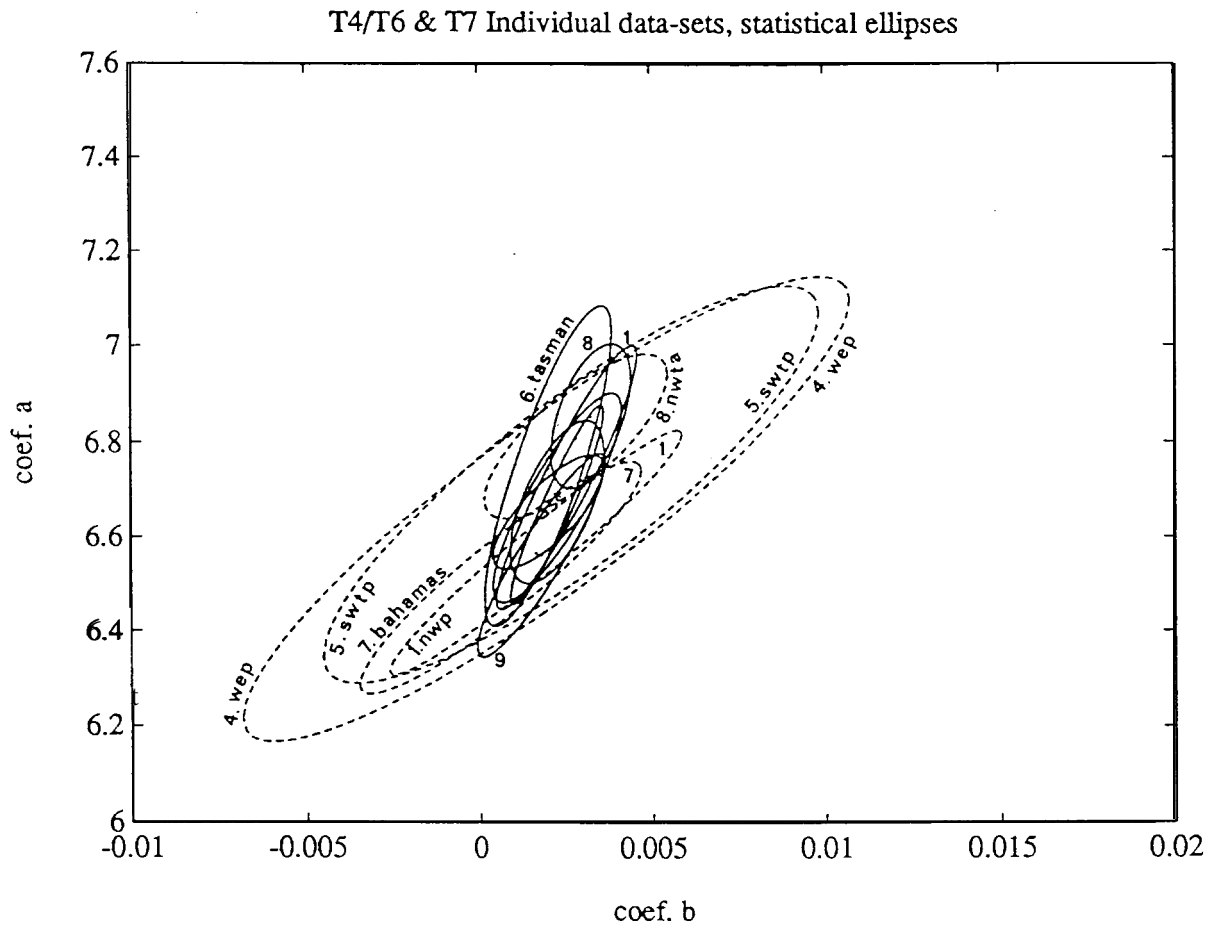
21

Figure 13   Individual regional 2-standard deviation ellipses on the *a-b* plane (95% confidence level; same scale as Fig. 6;   see Fig. 1 and Table 1 for the location of the regions). The full and the dashed ellipses are, respectively, the T-7 and the T-4/T-6 individual regional ellipses. For clarity, in the central group, some ellipses are referred to by their region number only.

6.3.3 *Probe manufacturer comparisons*

Probes from two different manufacturers were used in this study. They should be identical as the TSK probes are made under licence from Sippican. The individual T-7 and the T-4/T-6 probes from each manufacturer are grouped together for comparison on the *a-b* plane in Fig. 11 (see also Table 2). The standard-error-of-the-mean ellipses (95%) show that the two T-7 data sets are quasi-identical. They have very close mean All points, and their variability is comparable: there are 42 TSK T-7 *ab* points and 83 Sippican *ab* points, so the axes of the mean ellipses should have a theoretical ratio of 2/3, which is the case. The Sippican T-4/T-6 probes are not significantly different from the T-7 probes, but there seems to be a problem with the TSK T-6 probes (17 probes). This problem cannot be a batch problem as the probes were launched during two different cruises **3** years apart. It cannot be a regional problem, as most of the TSK T-7 probes were launched in the same area and sometimes during the same cruise with the same onboard equipment. There seems to be a real but small difference between the TSK T-6 XBTs and the other probes: -6m, or -1 .3%, maximum depth-error with the reference AB_{467} point.

6.3.4 *Discussion on the inter-comparisons*

Of the regional groups described above (Fig. 9), only the slow fall rate for TSK T-6 *(nwp)* may be explained by a statistically significant manufacturing difference. The location of the Bahamas data set in the slow fall rate group cannot be explained by density or viscosity effects, as one would expect these effects to result in it being in the medium fall rate group. As it is a single experiment using the same type of probes and onboard equipment used to collect some of the other data sets, the more plausible explanation is probe batch variation. Similarly, the north-eastern Atlantic data set *(nea)* is a single experiment, so its slow fall rate may be due to probe batch variations or, since it is the only experiment to use a Sippican Mk-12 onboard unit, it may be due to an onboard equipment influence. But since the high density and viscosity in the area favour a slow fall rate, this may be a regional influence. The high fall rate and the large mean ellipse of the Tasman sea single experiment, on the other hand, may be a batch problem plus the fact that the area of the experiment actually spans over subtropical and mid-latitude frontal regions. The high fall rate of the two T-7 and T-4/T-6 north-western tropical Atlantic *(nwta)* data sets cannot be explained by any influence. It is a multi-cruise, multi-onboard equipment, multi-institution, multi-probe experiment, and the density and viscosity in the area favour a medium fall rate. So, if this high fall rate is real, it is due to an influence of unknown origin.

Therefore, only two differences between the data sets cannot be explained by batch variations: *i)* The TSK T-6 probes systematic slower fall rate; *ii)* The north-western tropical Atlantic data set's high fall rate. However, these two differences have a very small influence on the overall combined data set, as the errors are symmetrical about the reference AB_{467} point (about ±6m or ±1 at 450m) and the TSK T-6 data sets constitute a small number of the comparisons evaluated. In fact, if all the regional *AB* points are plotted on the global AB_{457} reference planes (Fig. 12 and Table 1), most of these points are inside or along the ±6m maximum absolute depth-error isoline (or 1.3%), except the Tasman Sea (+10m) and the north-eastern Atlantic *(nea,* -9m). This is the maximum induced depth-error if the regional depth-time equations are replaced by the new reference depth-time equation (9). It is well within the scatter of the individual probes (within the 'individual' l-standard deviation ellipses of Fig. 8).

Moreover, if some differences were found in the means, all these differences are of practically no importance compared to the individual, or batch to batch, scatter of the probes (Fig. 13). All the 'individual' regional two standard deviation ellipses intersect to the extent that the slow and fast fall rate groups are hardly discernible. So, if any other influences do exist, they are embedded in the individual or batch-to-batch fall rate variations of the XBT probes. Unless the manufacturers are able to reduce that variability, further regional experimentation will not be of interest, except perhaps in extreme oceanic conditions of density and viscosity.

23

6.4 Observed variability and the manufacturers' specifications

In order to study the depth-errors over the whole water column and not only the maximum depth-error, one has to use the depth-error versus depth plane instead of the *a-b* plane. Figure 14a shows the distributions of the 5895 valid depth-differences as a function of their CTD depth (as calculated in *step 4)* for the combined T-4/T-6/T-7 data set. The elapsed times corresponding to the depth-differences are identical for each profile, as the depth-differences are determined every 25 "XBT metres" using the manufacturers' depth-time equation (6) in *step 1*. Therefore all the depth-differences at a given elapsed time can be grouped together to determine the depth-difference statistics for that given time (XBT depth). The corresponding CTD actual depths vary, as they are equal to the XBT depth plus the depth correction.

At each level the distribution of the depth-differences are quasi-normal and only a slight asymmetry in the scatter can be noted towards the high fall rate side of the distribution (high negative individual depth-error dots). The data are generally outside the manufacturers' specifications, except close to the surface where the mean depth-error is within $\pm 5m$ down to a depth of 150m. The mean depth-errors range from -2.5m at 100 metres to -24.5m at 775m. Only the very slow fall rates outside -1 standard deviation (about $15°/0$ of the data) are within the specifications almost down to the maximum depth. The observed scatter is much larger than expected from the manufacturers' specifications.

When the new T-4/T-6/T-7 equation (9) is used (Fig. 14b) instead of the original manufacturers' equation (6), the mean depth-error is greatly reduced and is now within ± 1 m of the CTD depth. However, 17.5% of the individual depth-errors are still outside the manufacturers' specifications (1028 depth-errors out of a total of 5895 depth-errors). Only the 1-standard deviation confidence interval is entirely within those specifications, and one must reach the maximum depth for the 2-standard deviation curves to be close to the specifications. Between 10Om and 500m, up to 30% of the depth-errors are outside the specifications.

A linear approximation of the 2 and 3 standard deviation curves (dotted lines in Fig. 14b) gives:

$$\pm (6m + 1.5\% \text{ of the depth }) \quad \text{for 2 std.dev. or 95.5\% of the data} \tag{10}$$
$$\pm (9m + 2.0\% \text{ of the depth }) \quad \text{for 3 std.dev. or 99.7\% of the data} \tag{11}$$

If the meaning of a specification is that the depths of all the probes should be within them, then the specifications provided by the manufacturers should be at least close to the 3-standard deviation confidence interval. They should be of the order of (11). It must be noted that the new specifications are not $\pm n$ metres or $\pm p\%$, but $\pm (n$ metres plus $p\%)$. The shallow depth specifications, therefore are much larger than they used to be; above $\pm 10m$ at $100m$ and around $\pm 15m$ at 250m instead of $\pm 5m$. Hallock and Teague (1992) found the same kind of probe-to-probe scatter after correction of the original data with their new equation: about ± 8 to 10 metres in the depth range 10m to 100m, and ± 15 to 20 metres in the range 450m - 650m.

The linearity of the standard deviation curves with depth is a good index of the reliability of the method used to calculate the depth-errors. All over the depth range, the relative scatter of the probes remains constant, about 1.5% of the depth at a 95% confidence level. Therefore, if the general behaviour of the probes with depth remains similar from probe to probe, the reliability of the method remains constant whatever the depth, even when the vertical temperature gradients change only slightly.

If, instead of the total 5895 depth-difference data set, we consider only the 5340 depth-differences used to determine the mean A_{467} and B_{467} coefficients of equation (9), the results are almost identical (not shown). Even the extreme data points (above 3-standard deviations in Fig. 14) are not eliminated, as they are part of some of the good profiles determined from more than 2/3 of the maximum number of depth-differences. The mean depth-error is still within ± 1 m, and the standard deviations are very slightly different, but the conclusions remain the same.
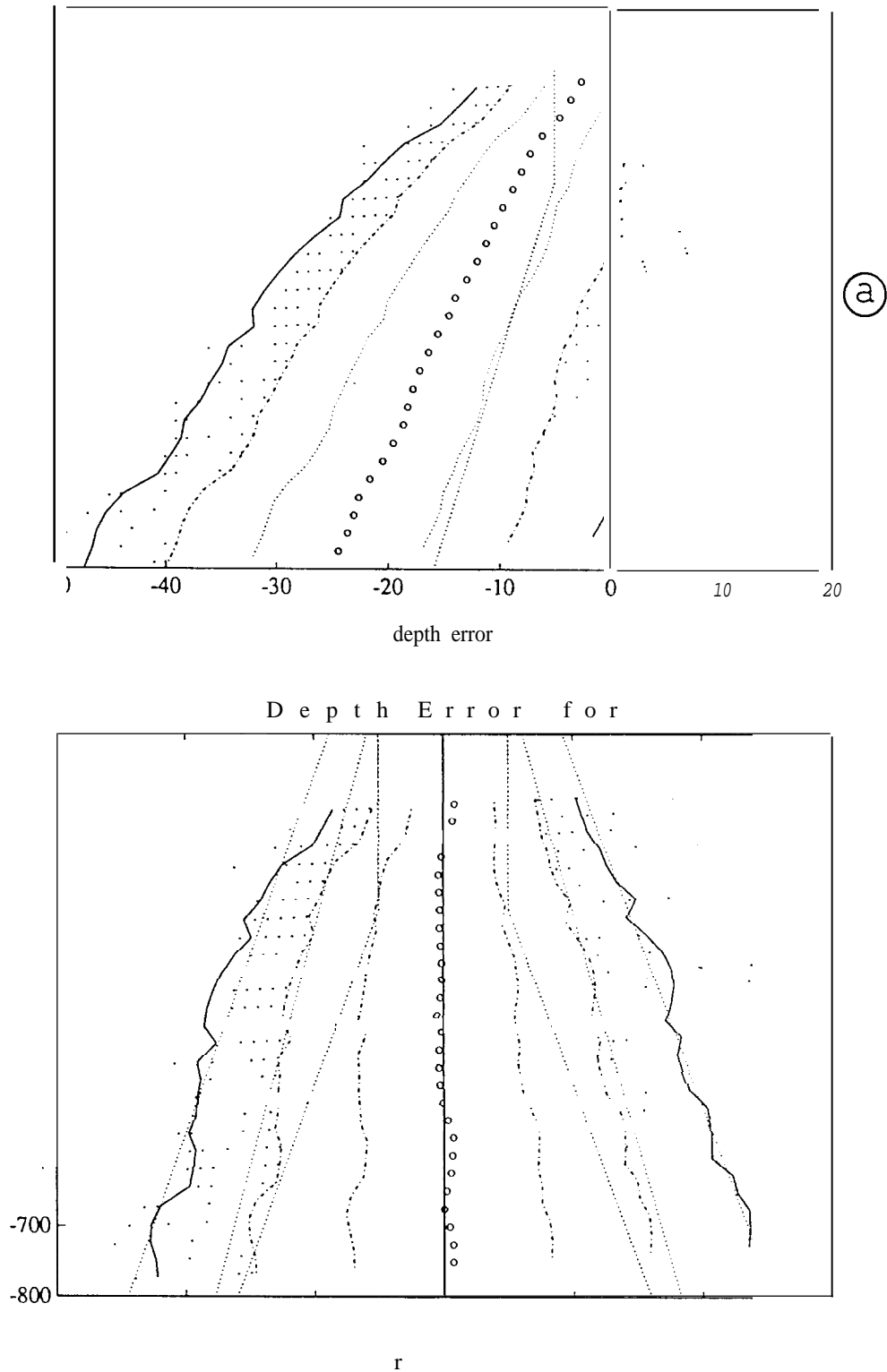
Figure 14 Combined T-4/T-6/T-7 data set: depth-errors and their statistics as a function of depth.

a) Using the manufacturers' depth-time equation (6): distribution of the 5895 valid depth-errors (calculated in step 4) as a function of their CTD depth. The mean depth-error (open circles) and the 1, 2, 3 standard deviations confidence intervals (respectively dotted, dash-dotted and full curves) are calculated independently for each XBT elapsed time (every 25 XBT metre). The individual depth-errors above two standard deviations (dots) are added. The manufacturers' specifications (±5m or *+2°/0* of the depth, whichever is the greater) are indicated as dotted lines.

b) Same distribution but using the new T-4/T-6/T-7 reference equation (9) instead of the manufacturer's equation (6). In addition linear approximations of the 2 and 3 standard deviation curves are indicated (dotted lines).

25

Table 3 Summary of previous XBT comparison experiments published by other investigators. Column 1 is the *ab* point number indicated in Fig. 15 or Table 3. Columns 3 is the publication year of the article. Column 11 gives the linear-correction coefficients used by several authors to correct the manufacturer's equation (6). The following columns are the linear *(A)* and quadratic *(B)* term of Eq. 5, plus, when existing, a constant term C (offset at the surface). The depth-error columns (col. 15 and 16) give the maximum absolute depth-error between the result of the new reference equation (9) and the author's result (down to 800m for the T-7 or to 450m for the T-4 probes and T-4-like T-7 experiments). The last two columns give, when necessary, the result of a re-calculation, by least square fit, of the author's 3-coefficient equation into a 2-coefficient equation of the form of equation (5),

n°	Author	Date	Nb. of XBT	Probe Type	Manu-facturer	Field Experiment Date	Field Experiment Area	XBT recorder	Depth Reference	Linear correct.	A 10^{-5}	B	C metres	Maximum depth-error metres	Maximum depth-error %	A 10^{-5}	B 10^{-5}
x	Sippican	1965		T4 T6 T7 DB	Sippican	?	?	?	?		6.472	216	-	-15 -15 -26 -26	-3.26 -3.26 -3.24 -3.24		
1	McDowell	1977	47	T7	Sippican	1976	Sargasso S.	Strip ch.	Plessey	1.020	6.601	220	-	-10.5	-1.3		
2s 2d	Heinmiller & al	1983	139	T7	Sippican	1976/78	Sargasso S.	Strip ch.	NB Is (1) (2)	0.995 1.044	6.440 6.757	215 226	-1.1 -17.1	-18.0 -9.5	-4.0 -1.1	6.367 6.350	108 -25
3	Singer	1990	14 15	T7 "	Sippican "	1985 1986	G.Mexico "	SA-810 Mk-9	NB III "	1.0435	6.754	225	-4.3	3.6	0.5	6.617	131
4	Henin	1989	35	T4	Sippican	1987	W trop. Pac.	Argos	SBE 9	1.050	6.796	227	-	7.1	1.6		
5	Sy &Ulrich	1990	11	T7 DB	Sippican	1989	Norw.Trench	SA-810	NB III	1.020	6.601	220	-	-10.5	-1.3		
6	Gould (3)	1991	29	T7	Plessey	1990	Iceland Faroes Ridge	SA-810	Echo-Sounder	1.050	6.796	227	-	12.8	1.6		
7	Hallock & Teague	1992	118	T7	Sippican	1990	Barbados	Mk-9	NB III	-	6.798	238	-4.0	7.3	0.9	6.669	149
8	Yoshida (4) & al	1989	22	T7	TSK	1988	Japan Sea	Z60II	NB IIIb	-	6.674	329	-	-6.1	-1.4		
9	Green (5)	1984	139	T7	Sippican	1976/78	Sargasso S.	Strip ch.	NB Is	-	6.450	131	-	-15.4	-1.9		

(1) linear correction from 0m to 325m
(2) linear correction from 326m to 760m
(3) true depth detected by a precision echo-sounder
(4) 0-300m XBT/CTD comparison (no temperature gradient below)
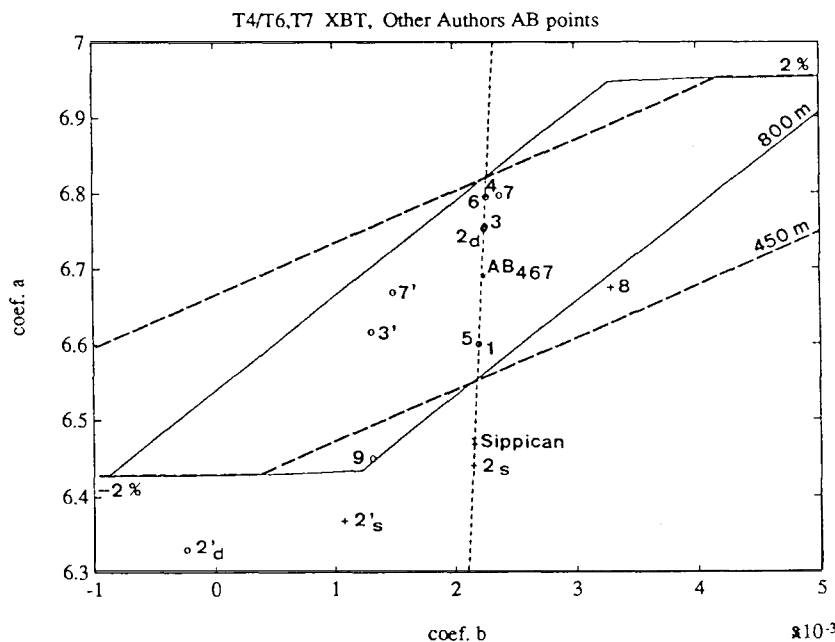(5) same data as Heinmiller & al, plus an hydrodynamic model

Figure 15 Other authors' results (see Table 3) on the *a-b* plane of the new T-4/T-6/T-7 reference equation (Eq.9; reference AB_{467} point marked by an *: $A_{467} = 6.691$, $B_{467} = 0.00225$; same scales as in Figs. 9 and 12): *i)* The other authors' mean *AB* points are numbered as in Table 3 column 1. Without consideration of the existence of a third constant term (2.s, 2d, 3, and 7), the circles are the T-7 *ab* points, while the crosses mark the T-4 or T-4-like T-7 *ab* points (2s and 8). The *ab* points numbered with a prime (2s', 2d', 3' and 7') are resulting from are-calculation of the 3-coefficient equations into 2-coefficient equations (see last. two columns of Table 3). The manufacturers' A_SB_S point is marked by an *(X)*. *ii)* The thick dashed and full line maximum absolute depth-error isolines are the ±2% isolines defined in Fig. 8, respectively, for the T-7 (800m) and T-4/T-6 (450m) *a-b* planes. The almost vertical thin dashed line is the $[00, A_SB_S]$ line, locus of any linear correction of the original manufacturers' equation (6).

26

7. Comparison with Other Authors' Depth-Time Equations

Singer (1990) made a comprehensive review of the articles published prior to his own publication. Table 3 is a summary of the latest major experiments known to the present authors. All of the experiments were XBT / CTD comparison experiments, except Gould (199 1) who compared the XBT depth when the probe hits the bottom to the depth of the bottom as measured by a precision echo-sounder reading. He also used Plessey T-7 probes which are not examined in our study, but which are supposed to behave the same way as the Sippican T-7 XBTs. The only other non-Sippican probe experiment was made by Yoshida *et al* (1989) who used TSK T-7 probes. Most of the probes are T-7 XBTs, except Henin (1989) who used T-4 XBTs. Yoshida's Japan Sea experiment was made down to a maximum depth of only 300m, so his TSK T-7 XBT results are more comparable to those for T-4 XBTs. The shallow (0-325m) linear correction from Heinmiller *et al.* (1983) can also be placed into the same group. The majority of the experiments were made at relatively low latitudes, although Sy and Ulrich (1990), Gould (199 1) and Yoshida *et al* (1989) made their measurements at higher latitudes in colder waters. No studies have been made in Arctic or Antarctic waters. The 1976-1978 Sargasso Sea experiments (McDowell, 1977, Heinmiller et al, 1983) where made using strip-chart recorders. Green (1984) used the same data as Heinmiller *et al.* (1983), but added an hydrodynamic model to define his 2-coefficient equation equivalent to (5).

The latest publications, Yoshida *et al.* (1989), Sy and Ulrich (1990), Gould (1991), Hallock and Teague (1992), used temperature-error-free methods to calculate the depth-errors. In the other publications, the authors tried to estimate the temperature error prior to the estimation of the depth error, and the result is accordingly less accurate. Another problem encountered in the earlier experiments is the non-exact simultaneity in time and/or space between the CTD and the XBT deployments, which allowed additional errors in the depth 'comparisons due to vertical displacement of features in the temperature field by internal waves and other high frequency space and time scale phenomena.

Table 3 also shows the maximum depth-differences between the previous authors' equations and the new reference T-7/T-4/T-6 depth-time equation (9). The maximum depth-differences for the T-7 experiments down to 800m are from +13m (1.6%) to -15m (-1 .9%). For the T-4's, or T-4-like T-7 experiments (cases 8 and *2s* don't go deeper than 325m, so they are considered in the T-4 group), the maximum depth-differences down to 450m are from +7m (1 .6%) to -6m (-1 .4%) and -18m (-4%) for *2s,* the worst case, very close to the manufacturers' equation.

In Fig. 15, the previous authors' results are presented on the *a-b* plane to show their relationship to one another and to the new AB_{467} reference point. Most of the earlier authors simply calculated a linear correction coefficient (like equation A2.8, Appendix 2) to correct the manufacturers' equation (6), thus the representative *ab* point is on a linear curve [00, $A_S B_S$] linking the origin of the *a-b* plane to the manufacturers' *AB* point. The Hal lock and Teague (case 7) *ab* point and our AB_{467} reference point, while differently determined, are nevertheless very close to the linear correction locus. The Yoshida (case 8) and Green (case 9) *ab* points have *b* coefficients far away from the linear correction curve. For the Yoshida case, this may be due to the special density structure of the Sea of Japan which has no temperature gradient below 300m. The maximum depth for comparison in that study is therefore 300m, and perhaps the quadratic coefficients can not be well defined due to the short depth-range. For the Green case, which uses the same data as Heinmiller *(2s and 2d),* it could be caused by a problem in a parameter evaluation of his model.

Several authors, who used the linear fit for their correction, also found at the surface an extrapolated offset of between -1 m to -17m (see Table 3). In order to be able to compare their results with the others on the *a-b* plane, we fitted a 2-coefficient equation (5) by the method of least squares to their 3-coefficient equation ($z= at -bt^2 +c$), thus eliminating the constant term c. The additional error due to this approximation is small; between -1 m and +2.5m in the depth range from 100m to 750m. The corresponding revised coefficients are given in Table 3. The original coefficients without the constant term are also presented in Fig. 15 for comparison.

Apart from the deep linear fit of Heinmiller *et al.* (Table 3, case *2d,* depth-range: 326m-750m), which gives a constant term of - 17m extrapolated to the surface, all the other offsets at the surface are in the range -1 m to -4.5m. Hallock and Teague (1992) and Singer (1990) discuss the issue of such offsets in more detail. Our results show no significant extrapolated offset near the surface (see Fig. 14b).

27

If the probes do behave differently close to the surface, we are unable to address the problem with our experiments and procedures as we did not define depth-difference information in the first hundred metres.

There seems to be no regional influence in the results from the previous authors. The identical 6 and 4 *ab* points are respectively in the cold North Atlantic and in the warm western tropical Pacific. The 1 and 5 *ab* points are also identical, but they are from the Sargasso Sea and from the Norwegian Trench respectively. Cases 3 and 7, which are very close, are from the western tropical Atlantic, but cases 1, 2s, 2d and 9 are also from the same area. There is perhaps a strip-chart recorder influence since all the corresponding *ab* points *(1, 2s, 2d, 9)* are in a slow rate group, but as they are also all from the Sargasso Sea this may be a regional effect. The other authors' results are generally about twice as far away from the AB_{467} reference point as our regional *AB* points (Fig. 12). This maybe due to probe batch variability, to differences in the methods or in the equipment, to the non-simultaneity of the launches, or sometimes to a regional variation as may be the case for the Sea of Japan data fromYoshidaetal.(1989).

In conclusion, most of the earlier authors' results fall within the ±2% depth-error isoline around our AB_{467} reference point. The exception is the Heinmiller *et al* (1983) result, but their data when re-interpreted by Green (1984) fall within the same ±2% envelope. Therefore our results do not contradict most of the previous results, but improve their accuracy and extend their applicability to a greater part of the world's oceans.

8. Depth Correction Formulas for Archived XBT Data

8.1 Full Correction Formula

In order to correct the depths of archived XBT data, we can calculate a correction formula where the new depth is a function of the original depth (see Appendix 2, equations. A2.5 and 6). If the original depth-time equation is the manufacturers' equation (6), and the new depth-time equation is the global T-4/T-6/T-7 equation (9) then, for the original depth z, the corrected depth Z is given by:

$$Z = 1.0417\, z - 75.906(\ 1\ -(1\ -2.063 10^{-4} z)^{1/2}) \qquad (12)$$

Figure A2.1 shows the depth correction applied to the original depth, which is about +15 metres at 450m, and +25 metres at 750m.

8.2 Linear Approximation Formula

The correction curve is almost linear so it is of interest to determine what kind of error is made by using a linear correction approximation. As the linear coefficients are a function of the maximum depth of the probe and of the type of maximum depth-error considered (see Appendix 2 for full details), there are two sets of linear coefficients. One set for the 800m maximum depth probe type (T-7), the other for the 450m maximum depth probe type (T-4/T-6). Each set is formed of three coefficients, one for each type of maximum depth-error: absolute, relative and absolute expressed as a relative depth-errors.
For the combined T-4/T-6/T-7 data set down to 800 meters, the best linear coefficients (see Appendix 2, equations. A2.10 to 12) are between 1.0336 to 1.0337 depending upon the depth-error considered, and between 1.0337 and 1.0338 down to 450 meters. In Fig. A2.3 are shown the depth-errors induced by the 800m coefficients. The archived data having no recorded probe type, it should be better to choose only one global linear coefficient for the T-4/T-6 and the T-7 probes. In order to minimise the absolute depth-error while keeping the relative depth-error within reasonable bounds in the first hundreds meters, the best linear approximation of the corrected depth could be:

$$Z_l = 1.0336\, z \qquad (13)$$

The maximum errors induced by using this linear coefficient are less than -0.lm at 800m for the T-7 probes, and less than 0.05m at 300m for the T-4/T-6 probes. The relative depth-error is less than ±0.03% for all depths. Thus the linear correction approximation is very accurate for these probes, but this

may not be true for other probe types and other manufacturers. For example, the scatter of the coefficients is wider for the T-7 data set alone (between 1.0330 and 1.0339, down to 800 meters), or for the T-4/T-6 data set (between 1.0330 and 1.0333, down to 450 meters).

9. **Conclusions and Recommendations**

Further evidence was found in this study that TSK and Sippican T-7, T-6 and T-4 XBT probes fall faster than the rate given by the manufacturers' depth-time equation, and that the resulting depth-errors are outside the manufacturers' specifications. The T-4/T-6 and the T-7 data sets were found not to be statistically different at the 95% confidence level. Therefore a unique new reference T-4/T-6/T-7 fall rate equation was conclusively determined by a temperature-error-free method applied to a number of XBT/CTD comparison data sets which were collected in three oceans and under controlled conditions. Unfortunately, there were no opportunities to collect comparison data sets in polar regions or other extreme oceanic conditions, No significant regional, onboard equipment, or probe manufacturer influence on the fall rate was detected, except perhaps a regional influence in the north-eastern Atlantic, and a manufacturing difference in the TSK T-6 probes. Any influences, if they do exist, are masked by the individual variability of the probes, especially of the T-4/T-6 probes. This variability is well outside the manufacturers' specifications, even when the mean depth-error is corrected to less than ± 1 m by using the new T-4/T-6/T-7 reference depth-time equation. The main source of XBT depth variability seems to be the probe-to-probe or batch-to-batch variability of the probes' characteristics. Unless the manufacturers are able to correct this problem, it will be useless to do more regional studies, except perhaps in the colder waters of high latitudes.

A review of the results published by previous investigators, which are generally from a single geographical area, leads to the same conclusions but with a larger variability . The previous methods used differ from one another, they were not all temperature-error-free methods, and the simultaneity of the XBT/CTD launches was not always respected. Temperature errors, as well as internal waves and/or other high frequency structures, may have influenced their results. Every effort was made in the present study to reduce such influences to a minimum.

It should be noted that the other types of Sippican/TSK probes, as well as probes produced by other manufacturers such as Sparton of Canada, will also need careful independent evaluation. It is important that each probe type (including different manufacturers) be evaluated to avoid inconsistencies occurring in the depth accuracies of XBT data stored in the national and international data centres. Indeed, until an international mechanism is established to implement general use of a new equation for the T-7, T-6 and T-4 XBTs, and until the equation used for depth determination, the probe type, and the probe manufacturer can be distinguished in the data archives, it is strongly advised that for the present time all XBT data sent to the national or international data centres include depths calculated from the original manufacturer's equation only. The existence of mixed data in the databases must be absolutely avoided.

Appendix 1

**Maximum Depth-Error Isolines and Statistics on the *a-b* plane
of the Coefficients for the XBT Depth-Time Equation**

If t is the time and a and b are all the possible coefficients of the XBT depth-time equation, a and b can be considered as two variables defining an *ab* plan; and one set of coefficients defines an *ab* point. If A and B are the true depth equation coefficients for a given probe type, and $a = A + \Delta a, b = A + \Delta b$ another set of coefficients used for the same probe type, then

$$Z \qquad = A\,t \qquad\qquad -\,B\,t^2 \qquad\qquad \text{is the true depth.} \qquad (1)$$
$$Z + \Delta z \quad = (A + \Delta a)\,t\,-(B + \Delta b)\,t^2 \qquad \text{is an approximated depth,} \qquad (2)$$
and
$$\Delta z \qquad = \Delta a\,t \qquad\qquad -\,\Delta b\,t^2 \qquad\qquad \text{is the depth-error.} \qquad (3)$$

Given values for the depth Z and the A, B coefficients, the time t can also be computed:
$$t = q - (q^2 - Z/B)^{1/2} \qquad\qquad \text{with } q = A/2B \qquad (4)$$

Maximum absolute depth-error

Since the depth-error Δz is a parabolic function of t, the magnitude of &7 is maximised either when the first derivative of Δz is equal to zero (at a variable depth Z_{eM}), or when the probe reaches its maximum depth $Z_M(t = t_M)$, (Fig. Al. 1). Hereafter these two types of depth-error will be labelled respectively first *derivative* and *deepest* depth-errors.

- *First derivative* depth-error:

$$d(\Delta z_M)/dt = O$$
implies
$$t_{eM} = \Delta a/2\Delta b \qquad\qquad \text{time of the first } \textit{derivative} \text{ error} \qquad (5)$$
$$Z_{cM} = (A - B\Delta a/2\Delta b)\,\Delta a/2\Delta b \qquad \text{is the corresponding depth} \qquad (6)$$
and
$$\Delta z_{eM} = \Delta a^2/4\Delta b \qquad\qquad \text{with } t_{eM} \text{ in the time-range } [0, t_M] \qquad (7)$$

It should be remarked that t_{eM} and thus Z_{eM} are dependent only upon the ratio $\Delta a/\Delta b$. Therefore the depth of the *first derivative* error is constant along any line centred on the *AB* point (iso-depth lines).

- *Deepest* depth-error:

$$\Delta z_M = \Delta a\,t_M - \Delta b\,t_M^2 \qquad\qquad (8)$$

- Maximum depth-error isolines:

The maximum depth-error is equal to the maximum of these two depth-errors when t_{eM} is within the time-range of the probe type, and otherwise it is always situated at the maximum depth. One can draw on the *a-b* plane, the isolines of that maximum depth-error (Fig. Al .2), Depending upon the position on the *a-b* plane an isoline i is expressed by i_1 or i_2, whichever is the greater:

from (7) $\qquad i_1 = \Delta a^2/4\Delta b \qquad$ or $\qquad \Delta b = \Delta a^2/4i_1$ or $\qquad \Delta a = \pm 2(i_1\Delta b)^{1/2} \qquad (9)$
$\qquad\qquad\qquad\qquad\qquad$ with $\qquad t_{eM} = 2i_1/\Delta a \qquad t_{eM}$ in $[0, t_M] \qquad\qquad (10)$

or from (8) $\qquad i_2 = \Delta a\,t_M - \Delta b\,t_M^2$ or $\qquad \Delta a = i_2/t_M + t_M\Delta b \qquad\qquad\qquad (11a)$
$\qquad\qquad\qquad\qquad\qquad$ and $\qquad \Delta b = \Delta a/t_M - i_2/t_M^2 \qquad\qquad\qquad\qquad (11b)$

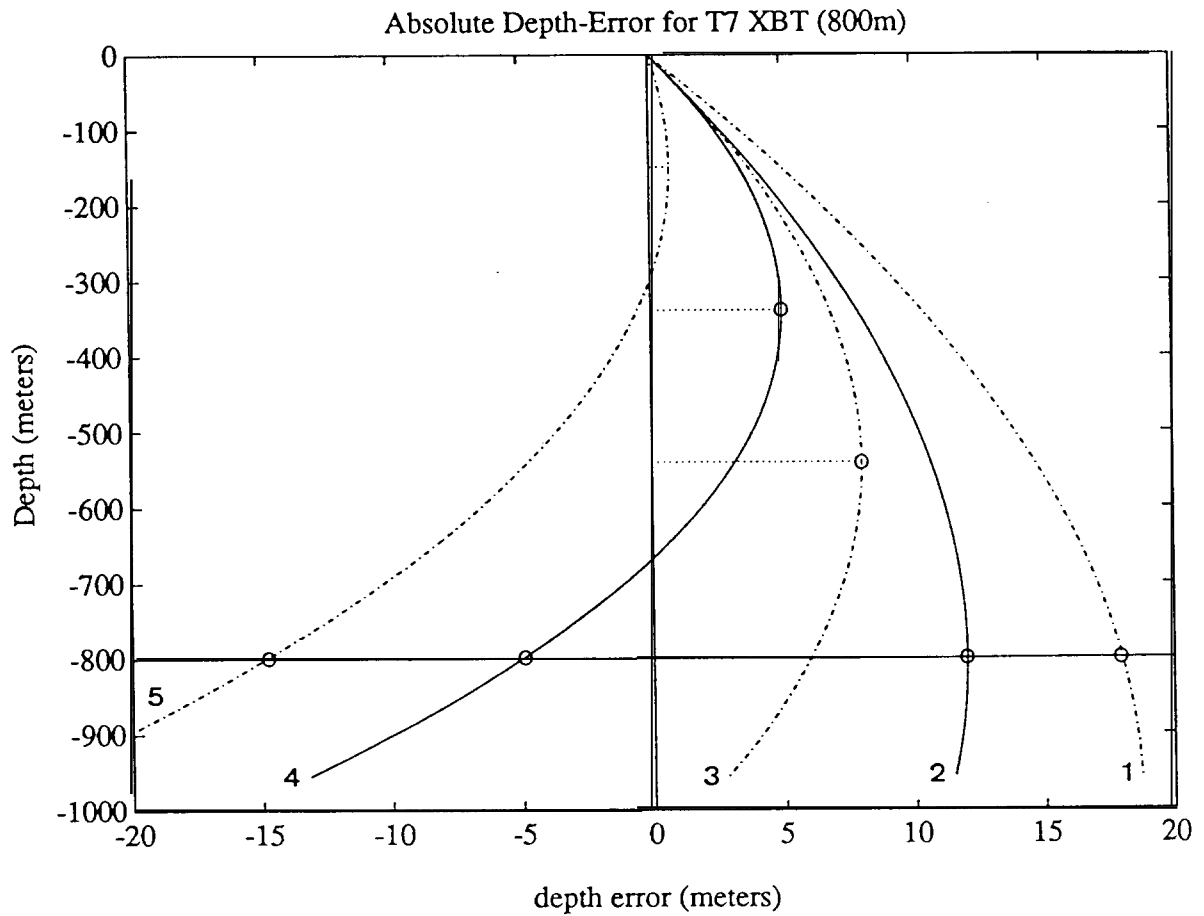## Absolute Depth-Error for T7 XBT (800m)

Figure A1.1:   Types of depth-errors for different sets of *a, b* coefficients (depth-time equation's coefficients of XBT probes). The maximum error may be located either at a depth Z_{eM} where the first derivative of the depth-error *(first derivative* error) is equal to zero (curve 3), or at the maximum depth Z_M accepted for the probe type *(deepest* error), here 800m, (curves 1 and 5). In curve 1 the *first derivative* error is outside the depth (time) range, while in curve 2 it is located at the maximum depth. In curve 4 the *deepest* error is equal to the *first derivative error,* but of opposite sign.

Maximum Absolute Depth-Error (meters) for T4/T6 probes (450m)

Maximum Absolute Depth-Error (meters) for XBT T7 probes (800m)

Figure A1.2:   Maximum absolute depth-error on the *a-b* plane (centred on the $A B_{467}$ point * of the new reference T-4/T-6/T-7 depth-time equation: A_{467} ̄ 6.691 and B_{467} ̄ 0.00225), for T-4/T-6 and T-7 probes:

   i) The full lines are absolute maximum depth-error isolines (equivalent to 1% of the maximum depth, 450m or 800m, for easy comparison with the following maximum relative depth-error figures).

   ii) The dotted lines *(T)* are the transfer lines where the *first derivative* depth-error is located at the maximum depth (450m or 800m).

   iii) The dash-dotted lines *(D)* are the discontinuity lines where the *first derivative error* (at $Z_{eM} = 189$m for T-4/T-6, or 340m for T-7) is equal to the *deepest* error (at 450m or 800m) but of opposite sign.

   iv) The upper right and lower left sectors (defined by these two lines) are areas where the *first derivative* error is the maximum depth-error, located at Z_{eM} (between 189m and 450m (T-4/T-6) or between 340m and 800m (T-7)). The two other sectors are areas where the maximum depth-en-or is the *deepest* error.

   v) The original manufacturer's equation *ab* point is marked by *o*. Its maximum depth-error for a T-7 probe is -26m at 800m. For a T-4/T-6 probe the error is -15m at 450m.

- <u>Transfer Line</u>:

By definition, the transfer line is the locus on the *a-b* plane where the *first derivative* error is equal to the *deepest* error. In the case of the absolute depth-error, this occurs only when the *first derivative* error is situated at the maximum depth (Fig. Al. 1, curve 2):

$$t_{eM} = \Delta a / 2\Delta b = t_M \quad \text{and} \quad Z_{eM} = Z_M$$

or
$$\Delta a = 2t_M \Delta b \tag{12}$$

This locus is a linear curve and it is the line where the maximum depth-error switches from the *deepest* error to the *first derivative* error (Fig. Al .2). The position of a given isoline *i* on the transfer line is:

$$\Delta a = 2i / t_M \quad \text{or} \quad \Delta b = i / t_M^2 \tag{13}$$

- <u>Discontinuity Line</u>:

There are positions on the *a-b* plane where the *first derivative* error is equal to the *deepest* error, but of opposite sign (Fig. Al. 1, curve 4):

$$\Delta a^2 / 4\Delta b = -(\Delta a - \Delta b\, t_M)\, t_M$$

or
$$\Delta a^2 + 4t_M \Delta b\, \Delta a - 4t_M^2 \Delta b^2 = 0 \tag{14}$$

All the points on the *a-b* plane having this property are solutions of the above equation. The only physical solution within the time range is :

$$\Delta a = 2t_{eM} \Delta b \quad \text{with} \quad t_{eM} = (2^{1/2} - 1)\, t_M \tag{15}$$

Along this line (Fig. Al .2), the two types of maximum depth-errors are of equal magnitude but of opposite sign, the first occurs at the maximum depth Z_M, the other at a lesser depth Z_{eM} constant for a given probe type (t_{eM} is only a function of t_M). This 1 line divides the *a-b* plane into a positive maximum depth-error area and a negative maximum depth-error area.

As the isolines are maximum amplitude depth-error isolines, this linear curve is a discontinuity line where the maximum depth-error changes sign while keeping the same amplitude. The position of a given isoline *i* on the discontinuity line is

$$\Delta a = 2i / t_{eM} \quad \text{or} \quad \Delta b = i / t_{eM}^2 \tag{16}$$

It should be noted that t_{eM} and therefore Z_{eM}, are independent of the isoline value. On, the discontinuity line the depth Z_{eM}, as well as the maximum depth Z_M, are constant. The discontinuity line is also the locus where the maximum depth-error is minimum for a given Δa or Δb or for a given distance from the reference point.

- <u>Sectors in the *a-b* plane</u>:

The transfer line and the discontinuity line, divide the *a-b* plane into 4 sectors centred on the reference *AB* point (Fig. Al .2). In the two smaller sectors where the isolines are more horizontal (top-right and bottom-left), the maximum depth-error is a *first derivative* depth-error, and occurs at different depths (Z_{eM}, for $t_{eM} = \Delta a / 2\Delta b$). These depths depend only upon the ratio $\Delta a/\Delta b$, therefore the depth is constant along any line centred on the *AB* point (the transfer line and the discontinuity line are part of this family). The maximum depth-error in the two other sectors always occurs at the maximum depth accepted for the given probe type (Z_M equals 450m for T-4/T-6 or 800m for T-7).
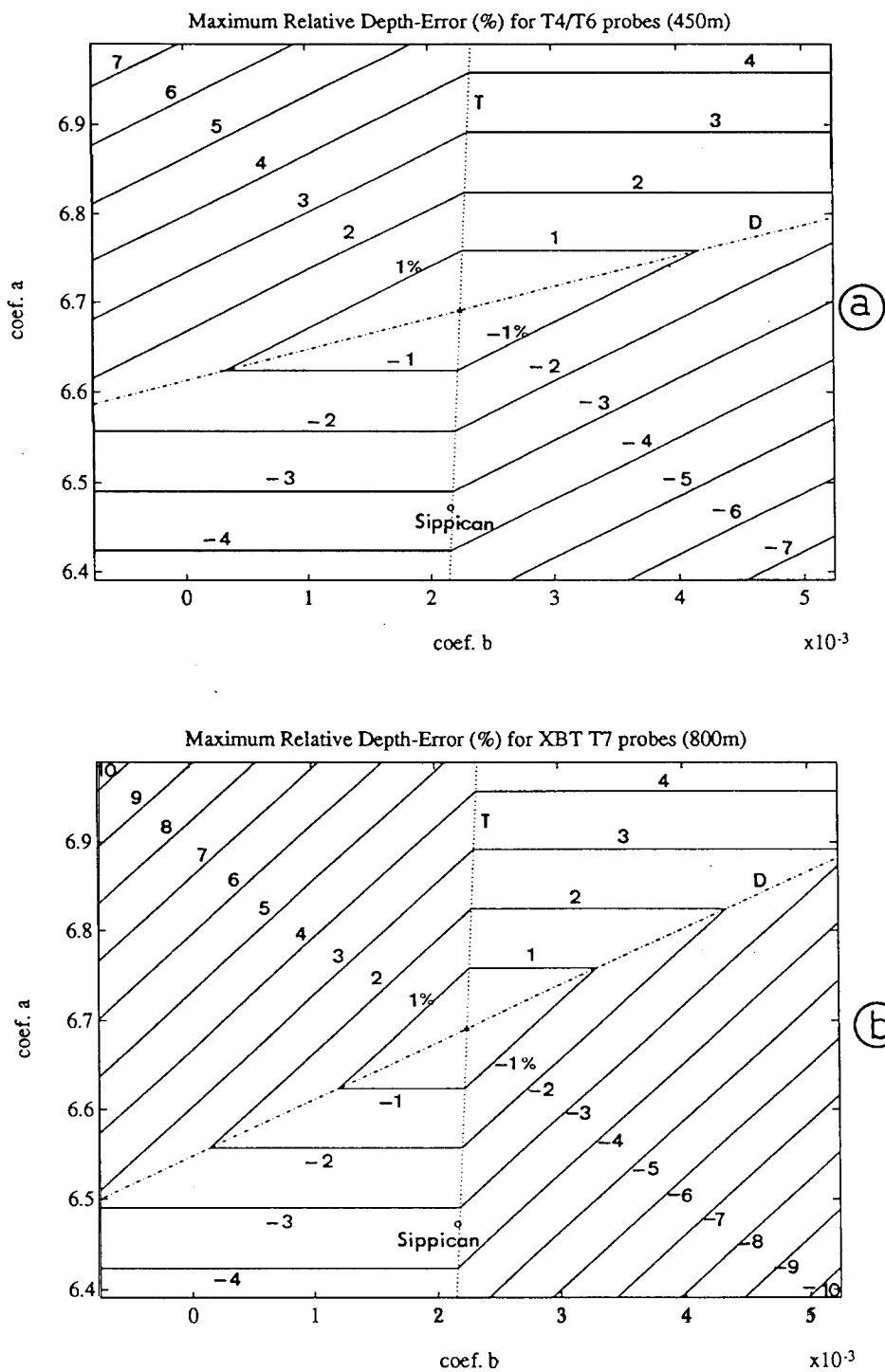
34

Figure A1.3: Maximum relative depth-error isolines on the same *a-b* planes as in Fig. Al .2:

     i) The full lines are maximum relative depth-error isolines. The relative depth-error is maximum either at the surface or at the maximum depth.

     ii) The dotted lines *(T)* are the transfer lines where the surface error is equal to the error at the maximum depth. The dash-dotted lines' *(D)* are the discontinuity lines where the surface error is equal to the error at the maximum depth but of opposite sign. The upper right and lower left sectors defined by these two lines are areas where the surface error is the maximum depth-error. The two other sectors are areas where the maximum depth-error is the *deepest* error.

     iii) The maximum relative depth-error of the original manufacturer's equation *ab* point, marked by o, is -3.26% at 800m. for a T-7 probe, and -3.24% at 450m for a T-4/T-6 probe.

The only *zero-error point* is the *AB* point at the centre of the plane, where Δa and Δb equal zero, but along the discontinuity line, the variation of the depth-error is minimum, as the depth-error curve is more or less symmetrical about the zero-error axis (Fig. Al. 1, curve 4). Thus the isolines define a central area, elongated along the discontinuity line, where the depth-error is small even when the *a b* coefficients are quite different from those of the reference equation.

Maximum Relative Depth-Error

The depth-error can be expressed as a relative depth-error (i.e. divided by its actual depth). In that case the relative depth-error is:

$$\Delta z \, / \, Z = (\Delta a - \Delta bt) \, / \, (A - Bt) \qquad \text{with } t \text{ in } [0, t_{\text{M}}] \qquad (17)$$

This hyperbolic equation is maximum either at the surface or at the maximum depth t_{M}, as the time satisfying the discontinuity condition $(t = A/B)$ *is* generally an order of magnitude greater than t_{M}. Hence the maximum relative depth-error is expressed by:

$$(\Delta z \, / \, Z)_0 \quad = \Delta a \, / \, A \qquad\qquad \text{at the surface} \qquad (18)$$

or
$$(\Delta z \, / \, Z_{\text{M}})_{\text{M}} = (\Delta a - \Delta bt_{\text{M}}) \, / \, (A - Bt_{\text{M}}) \qquad \text{at } Z_{\text{M}}, \text{ with } t_{\text{M}} << A/B \qquad (19)$$

The equation for an isoline *i* is either:

$$\Delta a = i \, A \qquad\qquad \text{maximum error at the surface} \quad (20)$$

or
$$\Delta a = i \, (A - Bt_{\text{M}}) + t_{\text{M}} \, \Delta b \qquad\qquad \text{maximum error at } Z_{\text{M}} \qquad (21)$$

depending upon the position on the *a-b* plane. The isoline is diamond shaped (Fig. Al .3), as both equations are linear. When the maximum error is at the surface, the isoline is parallel to the *b* axis.

Following the same definitions as in the above maximum absolute depth-error:

the transfer line is: $\qquad\qquad\qquad\qquad\qquad \Delta a = A \, \Delta b \, / \, B \qquad\qquad (22)$

and the discontinuity line is: $\qquad\qquad\qquad \Delta a = A \, t_{\text{M}} \Delta b \, / \, (2A - B \, t_{\text{M}}) \qquad (23)$

the intersection of an isoline *i* with the transfer line is: $\Delta b = i \, B \qquad \Delta a \; = \; iA \qquad (24)$

and the intersection with the discontinuity line is: $\qquad \Delta b = i \, (B - 2A \, / \, t_{\text{M}}) \qquad \Delta a = - \, iA \qquad (25)$

Maximum Absolute Depth-Error Expressed as a Relative Error

The relative depth-error, when maximum at the surface, represents a very small absolute depth-error at shallow depths. Thus a more useful compromise is to express the two maximum absolute depth-errors relative to their actual depth:

$$\Delta z_{\text{eM}} \, / \, Z_{\text{eM}} = \Delta a \, \Delta b \, / \, (2A \, \Delta b - B \, \Delta a) \qquad \text{with } t_{\text{eM}} \text{ in } [0, t_{\text{M}}] \qquad \textit{first derivative} \text{ error} \quad (26)$$

or
$$\Delta z_{\text{M}} \, / \, Z_{\text{M}} = (\Delta a - \Delta b \, t_{\text{M}}) \, / \, (A - Bt_{\text{M}}) \qquad\qquad\qquad \textit{deepest} \text{ error} \qquad\qquad (27)$$

The relative *deepest* error is identical to the relative error at the maximum depth, but the relative *first derivative* error is situated at Z_{eM} (generally below 100m) rather than at the surface, and it represents a significant depth-error (maximum of the absolute depth-error, see Fig. Al. 1, curves 3 and 4).
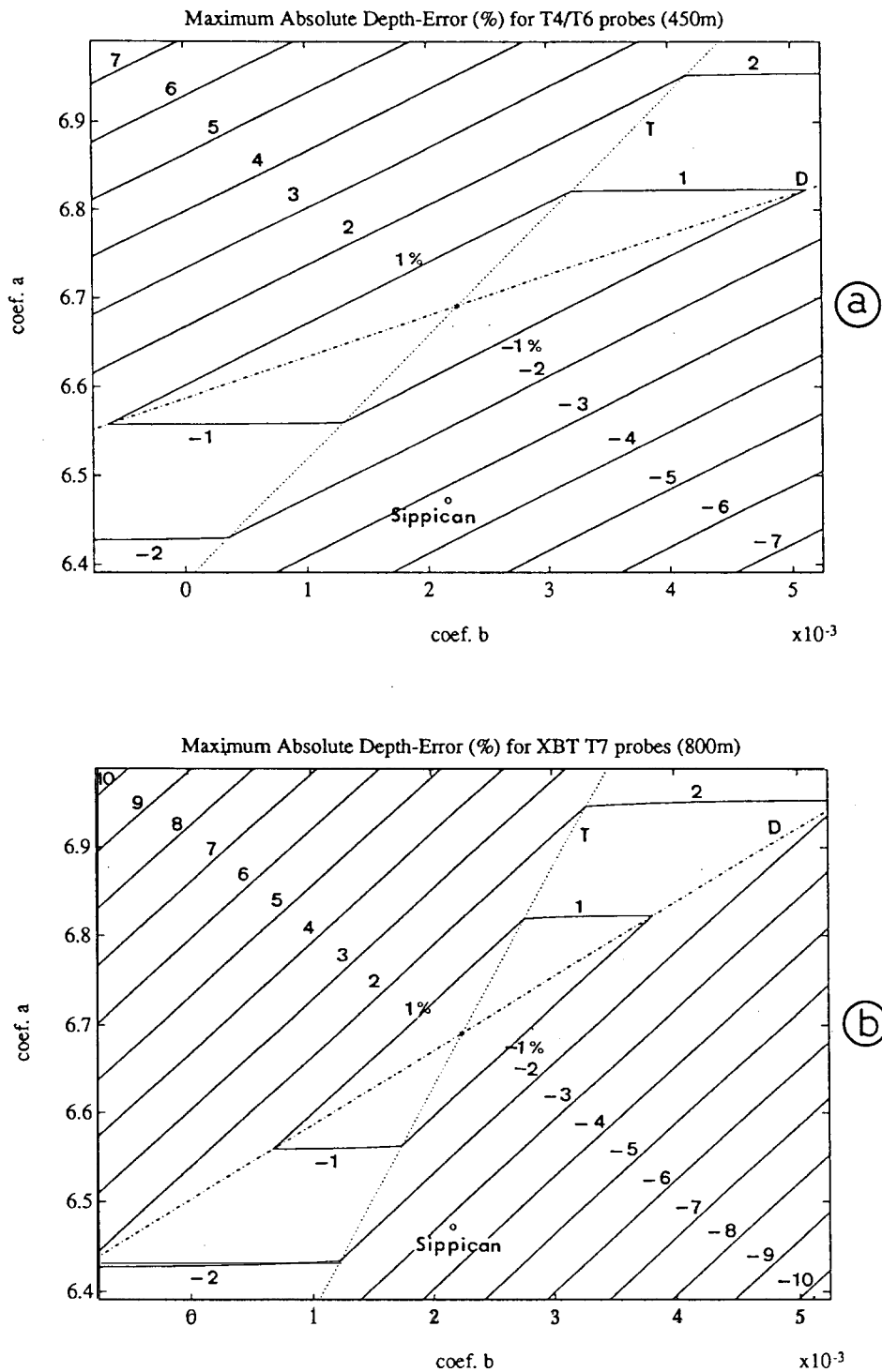
Maximum Absolute Depth-Error (%) for T4/T6 probes (450m)

(a)

Maximum Absolute Depth-Error (%) for XBT T7 probes (800m)

(b)

Figure A1.4: Maximum absolute depth-error expressed as a relative error on the same *a-b* planes as in Fig. A1.2: *i)* The full lines are absolute maximum depth-error isolines, expressed in percentage of the depth at which the error occurs.

   ii) The dotted lines (7) are the transfer lines where the relative *first derivative* depth-error is located at the maximum depth (450m or 800m). The dash-dotted lines *(D)* are the discontinuity lines where the relative *first derivative* error (at $Z_{eM} = 153$m (T-4/T-6) or 277m (T-7)) is equal to the relative deepest error (at 450m or 800m) but of opposite sign. The upper right and lower left sectors (defined by these two lines) are areas where the relative *first derivative* error is the maximum depth-error, located at Z_{eM} (between 153m and 450m (T-4/T-6) or between 277m and 800m (T-7)). The two other sectors are areas where the relative *deepest* error is the maximum depth-error.

   iii) The maximum depth-error of the original manufacturer's equation *ab* point, marked by *o.,* is identical to that of Fig. Al .3.

37

If i is an isoline value (Fig. A1.4), then these equations can be transformed to :

$$\Delta a = 2i\,A\,\Delta b\,/\,(iB + \Delta b)$$

first derivative isoline, (t_{eM} in $[0\ t_M]$) (28)
with a singularity at $\quad \Delta b = -iB$
and an asymptote for $\quad \Delta a = 2iA$

or $\qquad \Delta a = i\,(A - B\,t_M) + t_M \Delta b$ $\qquad$ *deepest-error* isoline $\qquad$ (29)

Following the same definitions as in the above maximum absolute depth-error:

the transfer line equation is: $\qquad \Delta a = 2\,t_M\,\Delta b$ $\qquad\qquad\qquad$ (30)
the discontinuity line equation is: $\qquad \Delta a = 2t_{eM}\,\Delta b$ $\qquad\qquad\qquad$ (31)
$\qquad\qquad$ with $\quad t_{eM} = (3 - (9 - 8B\,t_M\,/\,A)^{1/2})\,A\,/\,4B$ $\qquad$ (32)
the intersection of an isoline i
with the transfer line is located at: $\qquad \Delta b = i\,(A/t_M - B)$ $\qquad \Delta a = 2i\,(A - B\,t_M)$ $\qquad$ (33)
and with the discontinuity line at: $\qquad \Delta b = i\,(A/t_{eM} - B)$ $\qquad \Delta a = 2i\,(A - B\,t_{eM})$ $\qquad$ (34)

On the *a-b* plane, the area enclosed by one of these isolines (Fig. Al .4), is twice as large as the area enclosed by the same isoline of the maximum relative depth-error (Fig. Al .3). This reflects the rapid increase of the relative depth-error in the first tens of meters, where the absolute depth-error is rather small.

Statistics on the *a-b* plane

- <u>Statistical ellipses of the individual *ab* point Modulation</u>

The cloud of the individual *ab* points, about the mean *AB* point, can be considered as the distribution of two correlated quasi-normal variables. The confidence interval of such a bi-variate normal distribution, is represented by an ellipse centred on the mean *AB* point (Fig. Al .5). The major axis of the ellipse lies along the line of least rectangle, and the equation of the ellipse is (Dagnelie, 1973, Papoulis, 1981, or any treatise on bi-variate statistics):

$$u^2 - 2ruv + v^2 = c^2 \qquad\qquad (35)$$

where r is the correlation coefficient between a and b, $\pm c$ are the intersections of the ellipse with the axes u and v, and $u,\ v$ are the normalised variables:

$$v = (a - A)\,/\,\sigma_a \qquad\qquad u = (b - B)\,/\,\sigma_b \qquad\qquad (36)$$

where σ_a, σ_b are the standard deviations of a and b, respectively. Equation (35), can be resolved in v :

$$v = ru \pm ((r^2 - 1)\,u^2 + c^2)^{1/2} \qquad\qquad \text{for } u \text{ in } [-c\,(1 - r^2)^{-1/2}\,,\,c\,(1 - r^2)^{-1/2}] \qquad (37)$$

For an ellipse n for which a is in the confidence interval $[A - n\sigma_a, A + n\sigma_a]$ and b in $[B - n\sigma_b, B + n\sigma_b]$ (or equivalently u and v are in $[-n, n]$), c^2 is defined as:

$$c^2 = n^2\,(1 - r^2) \qquad\qquad (38)$$

The confidence level of the area enclosed by ellipse n, may be determined by referring to tables of the cumulative bi-variate normal density function such as those found in Abramowitz and Stegun (1972), Formery (1963), Lowe (1960), Owen (1956 and 1962), or Zelen and Severo (1960). For n<2, the confidence level is dependent upon the correlation coefficient r, but if $r \geq 0.5$ and $n \geq 2$, then the confidence level is very close to the confidence level of a single normal variable (95% for n = 2, 99.7% for $n = 3$, etc.).
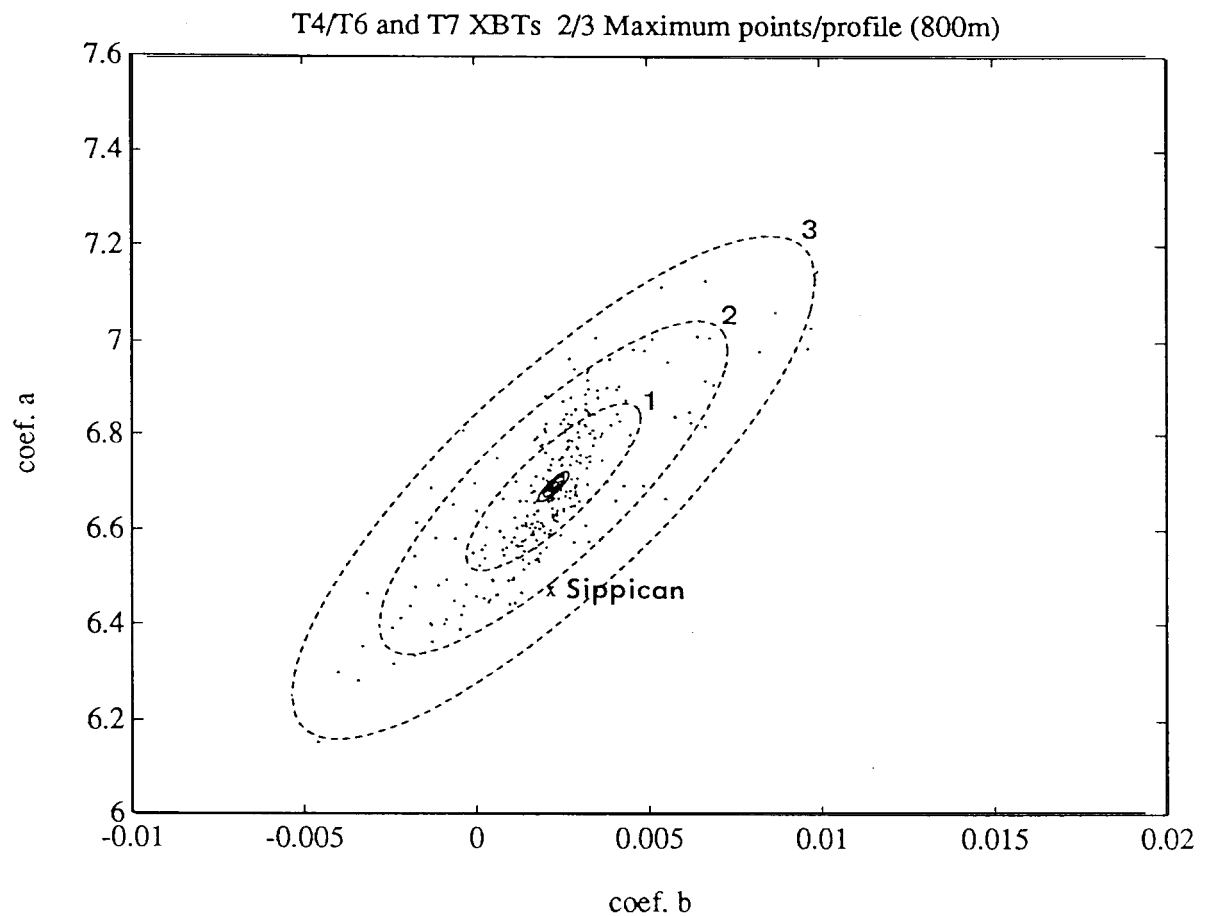
T4/T6 and T7 XBTs 2/3 Maximum points/profile (800m)

Figure A1.5:   Statistics on the *a-b* plane:

   i) The dots are the 285 T-4, T-6 or T-7 individual *ab* points used to calculate the new T-4/T-6/T-7 reference depth-time equation ($A_{467} = 6.691$ and $B_{467} = 0.00225$) The original manufacturer's equation *ab* Point is marked by (X).

   ii) The dashed ellipses are the confidence intervals, at 1, 2, 3 standard deviations, of the individual a_i and b_i around the mean AB_{467} reference point. The correlation coefficient between a's and b's is 0.83, therefore their confidence levels are, respectively, 58% (and not 68%), 95% and 99.7%.

   iii) The full small ellipses are the confidence intervals, at 1, 2, 3 standard-errors-of-the-mean, of the AB_{467} reference point. The confidence levels are the those of the individual ellipses.

- <u>Statistical ellipses of the mean *AB* point population</u>

Because the statistical distribution of a mean is closer to normal than the original distribution, these standard deviation ellipses can also be used to represent the confidence intervals of the mean *AB* points (Fig. Al .5). For the same confidence levels and a number of *ab* points *N,* the standard deviations to consider are the standard errors of the means:

$$\sigma_A = \sigma_a / N^{1/2} \qquad \sigma_B = \sigma_b / N^{1/2} \qquad\qquad (39)$$

Appendix 2

Depth Correction Formula for Archived XBT Data

Full Correction

In order to correct the depth for archived XBT data, we must find a correction equation where the new depth is a function only of the original depth. If z is the original depth stored with the archived data, and Z is the new corrected depth, while t is the **time, then** :

$$z = a\ t\ - b\ t^2 \qquad \text{is the original equation,} \qquad (1)$$
$$Z = A\ t - B\ t^2 \qquad \text{is the new corrected equation.} \qquad (2)$$

In order to find a transfer function $Z = f(z)$, the time $t = (aZ - Az)/(bZ - Bz)$ has to be eliminated and the final second order equation becomes:

$$b^2 Z^2 + (\ a^2 B - abA - 2bBz\ )\ Z + z\ (\ bA^2 - aAB + B^2 z\ ) = 0 \qquad (3)$$

After some transformations, the solutions to (3) can be written as:

$$Z = c_1 z + c_2 (\ 1 \pm (1 - c_3 z)^{1/2}) \qquad (4)$$

where $\qquad c_1\ B\ /\ b, \qquad c_2 = (A - aB\ /\ b\ )\ a\ /\ 2b, \qquad c_3 = 4b\ /\ a^2 \qquad (5)$

The only physical solution is one for which Z is positive and of the order of z (Fig A2.1). With c_1, c_2, c_3 of the order of 1, 10^2 to 10^4, and 10^{-4}, respectively, one can easily see that, in (4), the negative root **solution** only has a physical meaning:

$$z = c_1 z + c_2 (1 - (1 - c_3 z)^{1/2}) \qquad (6)$$

Since the original depth z is less than 100Om, $c_3 z$ is always less than 1 and the square root is always positive, but c_1 and c_2 are defined only for $b \neq$ zero.

If $b = O$ then (1) and (2) become:

$$z = at \qquad \text{thus} \qquad b = 0 \text{ implies } t = z\ /\ a$$
$$\text{and} \qquad Z = A\ t - B\ t^2$$
$$\text{or} \qquad Z = Az\ /\ a - Bz^2\ /\ a^2 \qquad (7)$$

Z becomes a function of the remaining coefficients and is then defined without ambiguity.

Remark: Another way to calculate the new depth Z is to extract t from (1) :
$$t = q - (\ q^2 - z\ /\ b\ )^{1/2} \qquad \text{with } q = a\ /2b$$
and then solve for Z, using (2).

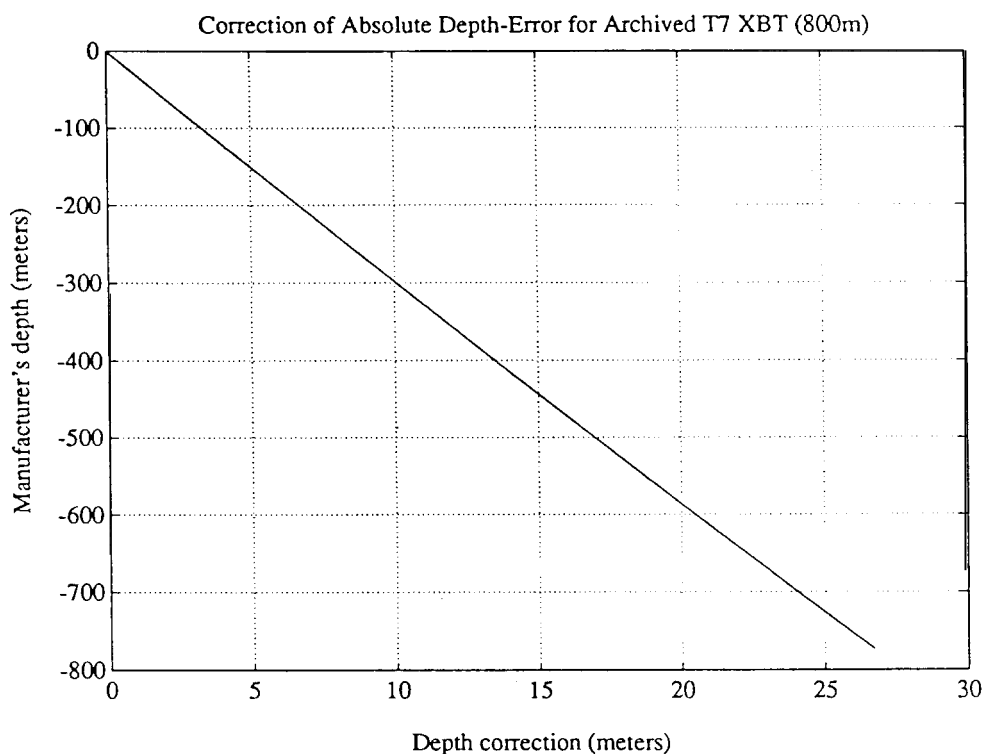**Correction of Absolute Depth-Error for Archived T7 XBT (800m)**

Figure A2.1: Full correction of the manufacturer's depth (depth-time equation's coefficients: $a = 6.472$, b = 0.00216), as a function of that depth. The new depth equation is the T-4/T-6/T-7 reference depth-time equation (coefficients $A = 6.691$, $B = 0.00225$).
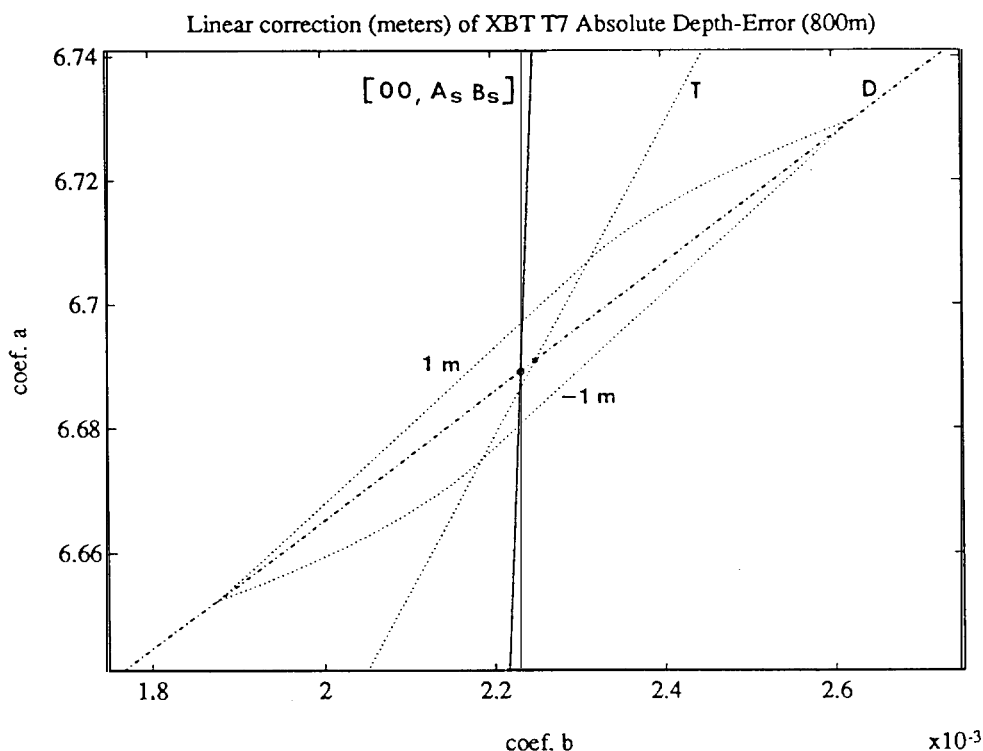
Linear correction (meters) of XBT T7 Absolute Depth-Error (800m)

Figure A2.2: Determination of a 'best' linear approximation's coefficient to correct the manufacturer's depth to the new reference depth (AB point *). On the a-b plane, the 'best' linear correction coefficient 1 is found at the intersection (o) of the [00 ab] full line locus of the linear corrections, with the discontinuity line (dash-dotted D line) locus of the minimum depth-errors. The dotted lines are the ±1m maximum absolute depth-error isolines and the transfer line (7).
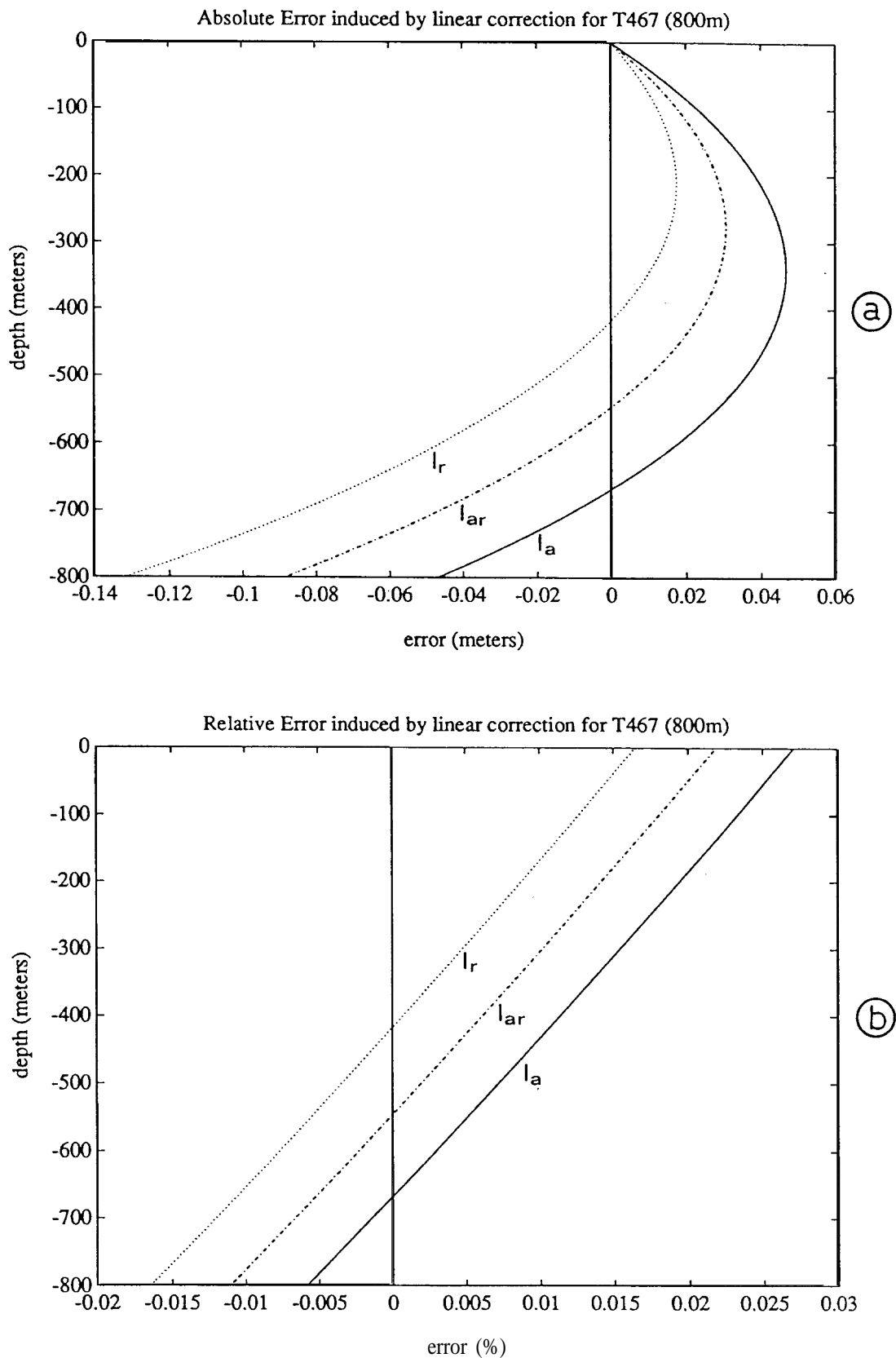
42

Figure A2.3: Depth-errors induced by a linear approximation of the full correction shown in Fig. A2.1. *i)* The upper figure shows the absolute depth-error induced by using the three 'best' linear coefficients calculated with the technique described in Fig. A2.2: absolute error coefficient (full l_a line), absolute error expressed as a relative error (dash-dotted l_{ar} line), relative error (dotted l_r line). *ii)* The lower figure shows the relative depth-error induced by using the same coefficients.

Correction by Linear Approximation

Since the full correction curve is nearly linear (Fig. A2.1), it is of interest to estimate the magnitude of the error made by using a linear correction approximation:

$$Z_1 = l\,z \qquad \text{where } l \text{ is a constant} \qquad (8)$$

or $\qquad Z_1 = l\,(a\,t\ -\ b\,t^2) \qquad$ where a, b are the original coefficients

if $\qquad \Delta a = l\,a - A$ and $\quad \Delta b = l\,b\ -B, \qquad$ where A, B are the new coefficients $\qquad (9)$

the error is $\qquad \Delta z_1 = \Delta a\,t\ -\ \Delta b\,t^2$

$l\ is$ unknown but, on the $a\text{-}b$ plane, the locus of $l\,(ab)$ is the line $[00,\ ab]$. On the other hand, as shown in Appendix 1, the maximum depth-error is minimised when an ab point is on the discontinuity line. Therefore, the best linear correction coefficient 1 is found when $l\,(ab)$ is at the intersection of the discontinuity line with the $[00,\ ab]$ line (Fig. A2.2). The maximum depth-error can be expressed as an absolute error or a relative error, each of these having its own discontinuity line. Therefore several 'best' linear coefficients can be computed by using the results from Appendix 1, and replacing Δa and Δb by their values (9):

-<u>Maximum absolute depth-error</u>:

$$\Delta a\ =\ 2t_{eM}\,\Delta b \qquad \text{discontinuity line (Al. 15)}$$

with $\qquad t_{eM} = (2^{1/2}-1)\ t_M \qquad$ where t_M is the time of the maximum-depth

so $\qquad l_a\ \ = (A - 2B\,t_{eM})\,/\,(a - 2b\,t_{eM}) \qquad\qquad\qquad (10)$

-<u>Maximum relative depth-error</u>:

$$\Delta a = A t_M\,\Delta b\ /\ (2A\ -\ B\ t_M) \qquad \text{discontinuity line (Al .23)}$$

so $\qquad l_r\ =\ 2A\ (A\ -\ B\ t_M)\ /\ (a\ (2A\ -\ B\ t_M)\ -Ab\ t_M) \qquad\qquad (11)$

-<u>Maximum absolute depth-error expressed as a relative error</u>:

$$\Delta a\ =\ 2t_{eM}\,\Delta b \qquad \text{discontinuity line (Al.3 1)}$$

with $\qquad t_{eM} = (\ 3 - (9 - 8B\ t_M/\,A)^{1/2}\ )\ A\ /\,4B$

so $\qquad l_{ar}\ \ = (A - 2B\,t_{eM})\,/\,(a - 2b\,t_{eM}) \qquad\qquad\qquad (12)$

These coefficients give their 'best' linear approximation by distributing the error more or less symmetrically (Fig. Al. 1, curve **4)**, with the magnitude of the error at the maximum depth equal, but of opposite sign, to the magnitude of the error at a higher level. The choice between these different 1 depends upon the result searched for. But l_{ar} seems to be a good compromise, reducing both the absolute and the relative errors, to a global optimum (Fig. A2.3).

References

Abramowitz, M., and A. Stegun, 1972: Handbook of mathematical functions, with formulas, graphs, and mathematical tables. Dover *Publications, New* York, 9th edition.

Bailey, R. J., H.E. Phillips, and G. Meyers, 1989: Relevance to TOGA of systematic XBT errors. *Proceedings of the Western Pacific International Meeting and Workshop on TOGA COARE, Noumea,* 1989. Edited by J. Picaut, R. Lukas, and T. Delcroix, Centre ORSTOM de Noumea, New Caledonia, 775-784.

Bailey, R. J., A. Gronell, H. Phillips, E. Tanner and G. Meyers, 1994: Quality control cookbook for XBT data. *CSIRO Marine Laboratories Report,* 221, 81 pp.

Blackman, R. B., and J. Tukey, 1958: The measurements of power spectra. *Dover Publications, New* York.

Brock, F.V., 1986: A non-linear filter to remove impulse noise from meteorological data. *J. Atmos. Oceanic Technol., 3, 51-58.*

Dagnelie, P., 1973: Théorie et méhodes statistiques. *Presses Agronomiques de Gembloux,* Gembloux, Belgique, pp 378.

Flierl, G. and A.R. Robinson, 1977: XBT measurements of the thermal gradient in the MODE eddy. *J. Phys. Oceanogr.,* 7, 300-302.

Formery, P., 1963: Integration de la distribution normale à deux variables dans un domaine polygonal. *Rev. Statist. Appl.,* 11 (2), 39-88.

Gould, W. J., 1990: Depth error in T-7s. *WOCE Newsletter,* 10, 10-11.

Gould, W. J., 1991: RRS Charles Darwin Cruise 50. *IOMSDL cruise report, 221,41* pp.

Green, A. W., 1984: Bulk dynamics of the expendable bathythermograph (XBT). *Deep Sea Res.,* 31,415-426.

Hallock, Z.R. and W.J. Teague, 1992; The fall rate of the T-7 XBT. J, *Atmos. Oceanic Technol., 9,* 470-483.

Hanawa, K. and H. Yoritaka, 1987: Detection of systematic errors in XBT data and their correction. *J, Oceanogr. Soc. Japan,* 32,68-76.

Hanawa, K. and Y. Yoshikawa, 1991: Re-examination of depth error in XBT data. J. *Atmos. Oceanic Technol.,* 8, 422-429.

Hanawa, K. and T. Yasuda, 1992: New detection method for XBT depth error and relationship behtween the depth error and coefficients in the depth-time equation. J. *Oceanogr.,* 48, 221-230.

Heinmiller, R. H., C.C. Ebbesmeyer, B.A. Taft, D.B. Olson and O.P, Nikitin, 1983: Systematic errors in expendable bathythermograph (XBT) profiles, *Deep Sea Res.,* 30, 1185-1196.

Henin, C., 1989: Experimental error of the expendable bathythermograph in the western tropical Pacific. *Paper presented at the first session of the TOGA XBT ad hoc Panel of Experts, Noumea, New Caledonia, June 1989,* pp 9 (unpublished manuscript).

Intergovernmental Oceanographic Commission, 1992: *Summary report on the Ad Hoc Meeting of the IGOSS Task Team on Quality Control for Automated Systems, Marion, Massachusetts, USA, 3-6 June 1991,* IOC/INF-888, pp 144.

Levitus, S., 1982: Climatological atlas of the world ocean. NOAA *professional paper* 13,173 pp.

Lowe, J. R., 1960: A table of the integral of the bivariate normal distribution over an offset circle. J. *Roy. Statist. Soc.,* ser. B 22, 177-187.

McDowell, S. ,1977: A note on XBT accuracy. *Polymode News, 29.*

Owen, D. B., 1956: Tables for computing bivariate normal probabilities. Am. *Math. Statist., 27, 1075-*1090.
Owen, D.B., 1962: *Handbook of statistical tables.* Pergamon press, London, pp 580.

Papoulis, A., 1981: Probability, random variables and stochastic processes, *McGraw Hill Int. Book Cy,* Tokyo, pp 583.

Rual, P., 1989: For a better XBT bathymessage, onboard quality control, plus a new data reduction method. *Proceedings of the Western Pacific International Meeting and Workshop on TOGA COARE, Noumea, 1989.* Edited by J. Picaut, R. Lukas, and T. Delcroix, Centre ORSTOM de Noumea, New Caledonia, 823-833.

Rual, P., 1991: XBT depth correction. *Addendum to the Summary Report of the Ad Hoc Meeting of the IGOSS Task Team on Quality Control for Automated Systems, Marion, Massachusetts, U. S. A., June 1991,* IOC/INF-888 Add, 131-144.

Seaver, G.A. and A. Kuleshov (1982): Experimental and analytical error of the expendable bathythermograph. *J Phys. Oceanogr.,* 12, 592-600.

Singer J. J., 1990: On the error observed in electronically digitized T-7 XBT data. J. *Atmos. Oceanic Technol.,* 7, 603-611.

Sy, A., 1985: An alternative editing technique for oceanographic data. *Deep Sea Res.,* 32, 1591-1599.

Sy, A. and J. Ulrich, 1990: North Atlantic ship-of-opportunity XBT programme - 1989 data report. *Wissenschaftlich- Technische Berichte aus dem Deutschen Hydrographischen Institut,* 1990-2, pp 89.

Sy, A., 1991: XBT measurements. *WOCE Operations Manual, Part 3.1.3 WHP Operations and Methods, WOCE Report,* 67/91, 19 pp.

Zelen, M., and N.C. Severo, 1960: Graphs for bivariate normal probabilities. *Ann. Math. Statist.,* 31, 619-624.

21	Bruun Memorial Lectures, 1979: Marine Environment and Ocean Resources	E, F, S, R
22	Scientific Report of the Intercalibration Exercise of the IOC-WMO-UNEP Pilot Project on Monitoring Background Levels of Selected Pollutants in Open Ocean Waters	(out of stock)
23	Operational Sea-Level Stations	E, F, S, R
24	Time-Series of Ocean Measurements. Vol. 1	E, F, S, R
25	A Framework for the Implementation of the Comprehensive Plan for the Global Investigation of Pollution in the Marine Environment	(out of stock)
26	The Determination of Polychlorinated Biphenyls in Open-ocean Waters	E only
27	Ocean Observing System Development Programme	E, F, S, R
28	Bruun Memorial Lectures, 1982: Ocean Science for the Year 2000	E, F, S, R
29	Catalogue of Tide Gauges in the Pacific	E only
30	Time-Series of Ocean Measurements. Vol. 2	E only
31	Time-Series of Ocean Measurements. Vol. 3	E only
32	Summary of Radiometric Ages from the Pacific	E only
33	Time-Series of Ocean Measurements. Vol. 4	E only
34	Bruun Memorial Lectures, 1987: Recent Advances in Selected Areas in the Regions of the Caribbean, Indian Ocean and the Western Pacific	Composite E, F, S
35	Global Sea-Level Observing System (GLOSS) Implementation Plan	E only
36	Bruun Memorial Lectures 1989: Impact of New Technology on Marine Scientific Research	Composite E, F, S
37	Tsunami Glossary - A Glossary of Terms and Acronyms Used in the Tsunami Literature	E only
38	The Oceans and Climate: A Guide to Present Needs	E only
39	Bruun Memorial Lectures, 1991: Modelling and Prediction in Marine Science	E only
40	Oceanic Interdecadal Climate Variability	E only
41	Marine Debris: Solid Waste Management Action Plan for the Wider Caribbean	E only
42	Calculation of New Depth Equations for Expendable Bathymerographs Using a Temperature-Error-Free Method (Application to Sippican/TSK T-7, T-6 and T-4 XBTs)	E only